36-45-41

DISPERSION OF HEAT AND HUMIDITY FROM ATMOSPHERIC SPRAY-COOLING SYSTEMS*

H. Weinstein, R. W. Porter, S. Chaturvedi,
R. A. Kulik and J. E. Paganessi
Illinois Institute of Technology
Chicago, Illinois 60616, U.S.A.

ABSTRACT

Spray cooling systems are alternatives to evaporative cooling towers for waste heat disposal of large electric power plants. In particular, visual appearance, noise, fog and drift may be more favorable. The present investigation includes field experiments, laboratory simulations and theoretical analysis of the so called base flow of the discharge.

A spray canal at Quad-Cities Nuclear Station (Illinois) was the subject of the field experiment. Both dry-and wet-bulb temperatures were monitored downwind of the canal. Both decayed with the -3/2 power of distance.

The laboratory simulation was carried out in an environmental wind tunnel. Helium was injected through several source simulation devices to represent the buoyant discharge. Three-dimensional maps of helium concentration were obtained along with measurements which characterize the incident and downstream boundary layers.

Results were evaluated using a fluid-dynamic convective-diffusion equation for the atmospheric surface layer.

INTRODUCTION

Spray cooling systems are alternatives to evaporative cooling towers for waste heat disposal of large electric power plants. In particular, visual appearance, noise, and drift may be more favorable. The discharge is spread over a larger area at the source and is closer to the ground. Because of the predominantly large 0 (cm) diameter drops of the subject sprays, drift loss is extremely small from the point of view of momentum and energy considerations. However, drift may be important where small amounts lead to icing and salt deposition in certain localities. A knowledge of the behavior of the base flow will

* Supported by NSF under Grant AER-74-01600 with technical management by ERDA, Conservation Division.

permit improved computation of drift trajectories and deposition and a determination of the occurrence of fog. A knowledge of dispersion is also important in terms of thermal performance where large-scale interference on down-wind segments may be possible depending on the system configuration.

The object of this study was to develop a laboratory simulation and an analytical model which after comparison with a field study for verification could be used to investigate a spectrum of possible operating conditions. Since the atmospheric flow and a power station's heat rejection requirements are both so variable it becomes at best an enormous task to investigate the whole range of possible operating states directly in the field. Therefore, the three component parts of this investigation were undertaken simultaneously and the results compared herein to determine best estimates of the important parameters of the discharge as power-law functions of the downstream distance.

Previous experimental studies of environmental effects of spray canals by other investigators as contained in the open literature are apparently restricted to consideration of drift. For example, drift for various drop sizes versus distance are given for a spinning-disc-rotor spray generator in [1]. Data for the Ceramic Cooling Tower Modules, discussed below, are given in [2, 3, 4]. However, as pointed out by Guyer and Golay [3], the trajectory of drift droplets is dependent on evaporation and condensation, variable aerodynamic drag due to plume behavior, and variations in ambient wind speed. It is thus important to have a good understanding of the flow containing the drift. Further, the effects of fog as well as heat and humidity are of general interest. These are especially sensitive to the so called base flow.

The surface layer of the atmospheric boundary layer has been studied in both field experiments and laboratory simulations in environmental wind tunnels. A discussion of atmospheric data and flow modelling in wind tunnels is given by Cermak, [5]. He gave the following criteria for the experimental simulation of the type undertaken here: An undistorted geometric scaling, equal Richardson numbers, "aerodynamically rough" surface roughness, similar surface temperature distribution, similar mean and turbulent velocity and temperature distribution. Since all these conditions can not be met simultaneously, a judicious choice must be made to simulate those scales of motion with the greatest significance for the present application. A discussion of the scaling laws for the simulation is given in the text.

A comparison of the experimental results is made with the analytical results of Rao, et al. [6] Their work is

interesting because of the sophisticated treatment of turbulent transport. Their work also compares well with Cermak's [7] Lagrangian analysis of plume dispersion which is used for comparison with the present results. Sutton's [8] analysis for point and line source dispersion yielded power law forms for ground level concentrations and these are also used for comparison in the text.

A 4-row-across spray canal at Commonwealth Edison Company's Quad-Cities Nuclear Station (Illinois) was investigated in the field experiment. The ambient atmospheric conditions were monitored at the 2-m height upwind of the system. The water temperature toward which the wet-bulb temperature is driven was also recorded. Both dry- and wet-bulb temperatures were monitored at the 2-m height downwind of the canal in the absence of fog. While the data are restricted to the "near field" where increments above ambient are appreciable, they are important for determining initial discharge behavior.

The laboratory simulation was carried out in a 43 x 46 x 214 cm environmental wind tunnel designed to simulate conditions that exist in the lower atmospheric surface layer. Injection of helium was made to simulate the buoyant discharge. The helium was introduced through a round orifice (point source simulation), a slit (line source), and a porous plate (also essentially a line source) which could be rotated to vary the angle of incidence of the approach wind. Measurements were made of the incident and downstream boundary layers which included turbulence intensity, Reynolds stress, macro and micro scales and velocity profiles. In order to characterize the simulated boundary layer, three dimensional maps of helium concentration, simulating air and water vapor, were also obtained downstream of the discharge. Spreading rates of the discharge were determined and compared to values found in the literature and the field studies.

An analysis of the spreading of the discharge was also carried out. The spray canal is modelled as a continuously distributed source of energy and moisture. Convective-diffusion equations for enthalpy and moisture are used with an NTU (Number of Transfer Units) model for the spray cooling. Numerical solutions of the resulting equation are compared to the experimental results.

FIELD EXPERIMENTS

Test Conditions

The Quad-Cities Nuclear Station of Commonwealth Edison Company (Illinois) uses a 4-row-wide spray canal which is about 60 m

across and 3 km long forming an oval loop. In the Richards of Rockford section, 56-kw motor pumps drive 4.5 x 10^4 l/min through single 16-m-diameter sprays of 5.2-m height in each of 152 floating modules. In the Ceramic Cooling Tower (CCT) section, 51-kw pumps drive 3.8 x 10^4 l/min through 4 12.2-m-diameter sprays of 5.5-m height in each of 176 modules. The spray layout is shown in Figure 1.

The segment analyzed was a continuous north-south run of 36 CCT modules. Under the particular test conditions, the water level was somewhat low and the bank height was 3.9 m with a 3:1 (horizontal:vertical) slope. Prevailing conditions averaged over the experiment included

date	8-6-75
time	12:25-15:54
ambient wind speed @ 2 m	3.7 m/s
ambient wind angle to canal @ 2m	79°
ambient wet-bulb temperature (WBT) @ 2 m	16.1C
ambient dry-bulb temperature (DBT) @ 2 m	22.8C
canal water temperature	36.8C
most upwind spray temperature (est)	33.9C
most downwind spray temperature (est)	35.2C
clear-day atmosphere	--

The ambient sensors were positioned 2 m over ground level, 50 m upwind of the canal and out of the influence of the sprays. The terrain was open grassland of about 0.5 m height of growth.

Instrumentation and Procedures

Wind run was sensed with a Gill low-threshold photo-chopper cup-type anemometer calibrated in the IIT 4 x 6 ft Environmental Wind Tunnel to be within 0.1 m/s. The output pulses were recorded on an event channel and later summed over the test interval to provide average wind speed. Wind direction was sensed with a Gill bivane with 1000-ohm potentiometer element. Wet-and dry-bulb temperatures were obtained using an Atkins aspirated psychrometer module with thermistor elements. The thermistors and bivane potentiometer were automatically sequentially sampled with several minutes dwell in conjunction with an Atkins thermistor bridge recording on an analog channel. A decade resistance substitution box was used to insure recorded temperatures within 0.1-C maximum error, the probe interchangeability tolerance. Wind direction was accurate within several degrees. The analog data were averaged over the sample duration to provide gust-integrated values which were then

tabulated for correlation in time with measurements made downwind of the canal.

The canal water temperature was stable as periodically verified by readings of an Atkins thermistor sounding probe and bridge. Canal water temperatures are very well mixed at a section [10] and also were accurate within 0.1C. The estimated spray temperatures were computed using parameters discussed in Reference [11] (NTU = 0.15, upwind f=0, downwind f = 0.45) from other experiments.

Two additional Atkins psychrometer modules with another sequential sampler, bridge and recorder were positioned downwind of the canal at the 2-m elevation. One psychrometer was fixed at a distance x_o = 41 m from the canal and spray centerline while the second was moved downwind in intervals. Recorded temperatures were also accurate within 0.1C.

Experimental Results

Data are correlated in terms of the dimensionless interference allowance [10-13]

$$f_{WB} = (T_{WB} - T_{WB\infty})/(T - T_{WB\infty})$$

where T_{WB} is wet-bulb temperature, ∞ denotes ambient and T is canal water temperature. Quantity $0 \leq f \leq 1$ as the ambient wind is driven toward equilibrium with the sprays. Also considered was the dry-bulb

$$f_{DB} = (T_{DB} - T_{DB\infty})/(T - T_{DB\infty})$$

Data are plotted in Figure 2 in ratio to respective f (x_o) values. They appear to fall off with the -3/2 power of distance from the spray centerline. A consideration of psychrometrics over small increments in state would show a similar f for specific humidity

$$f_w = (w - w_\infty)/(w_s(T) - w_\infty)$$

where "s" denote saturation, would fall off in the same manner in ratio to the value at x_o.

LABORATORY STUDIES

Experimental

The laboratory simulation was carried out in a 43 x 46 x 214 cm environmental wind tunnel designed to simulate typical conditions that exist in the lower atmospheric boundary layer.

The wind tunnel is shown in schematic form in Figure 3. Injection of helium was made to simulate the buoyant discharge. The helium was introduced through a round 0.635 cm diameter orifice (point source simulation), a 0.056 cm x 38 cm slit (line source), and a 2.54 cm x 30.5 cm porous plate mounted flush with the tunnel floor (also essentially a line source) which could be rotated to vary the angle of incidence to the approach wind. These three injection devices are shown in Figure 4.

The tunnel inlet section is packed with 0.3175 cm x 25.4 cm soda straws to provide a uniform flow and to damp room air turbulence levels. The inlet section is followed by a 91.5 cm section to generate a smooth boundary layer flow. The test section is also 91.5 cm long with a 31 cm gear rack traversing mechanism attached axially to the top wall. This top wall could be moved in the tranverse direction. With this configuration, a probe could be positioned anywhere in the test section.

At the entrance to the initial section, a 5 cm diameter counterjet tube was fixed just below the floor of the test section. This counterjet device is a modification of one discussed in reference [9]. The tube was drilled across the entire width of the tunnel with 0.32 cm holes. Air was injected through the counterjet device to establish a thicker boundary layer. Longitudinal roughness strips were added along the tunnel floor when the counterjet device was in use.

The instrumentation consisted of a two channel hot wire anemometer system with hot film probes. Helium concentration was measured directly with an aspirating hot film probe manufactured by Thermo-Systems, Inc. In the region of pure air flow, measurements could be made of mean velocity, axial and vertical turbulence intensities, Reynolds stress, and micro and macro scales of turbulence. In the two-component region, mean velocity and mean concentration could be measured.

It was intended to simulate the fully developed or equilibrium atmospheric boundary layer in the wind tunnel. In order to do this, the thick boundary layer generated in the tunnel must be in equilibrium. This means that the velocity profile shape, turbulence properties, etc., do not change in the streamwise direction. This was not the case with the boundary layer generated in the tunnel wherein a counter wall jet at the intake was used to shape the profile. However, the boundary layer generated did simulate many aspects of real atmospheric layers. The actual laboratory boundary layers in equivalent characteristics ranged from slightly unstable-to-neutral, to stable-to-neutral conditions, depending on the case.

Typical boundary layer profiles are shown in Figures 5-8. Figure 5 shows the boundary layer profiles for 5 axial positions in the test section. It is seen that the power law exponent, n, varies from about 5 to 3 with distance downstream. The streamwise and vertical turbulence intensities for the same case are shown in Figures 6 and 7. The variation through the boundary layer is as expected and there is relatively little variation with axial position. Figure 8 shows the Reynolds stress variation (friction velocity squared) through the boundary layer. There is a region of relatively constant U_*^2 near the wall with a relatively large amount of scatter in the data. A summary of the boundary layer parameters for all the cases studied is presented in Table 1. Since the experiments were done in two stages, the data are so presented. Stage I refers to the point and line source experiments. After installation of the porous plate source, it was found that the modifications slightly changed the wind tunnel operating point and data with this source are called Stage II data.

The Stage I measurements show some internal inconsistencies in that the frictional velocity, U_* is independent of roughness for the point source case. While for the line source data U_* does depend on roughness. The line source U_* without roughness is about the same as that for the point source cases but the line source U_* with roughness is much larger. The velocity profile shape parameter n should decrease with increasing roughness and again this is clearly shown in the line source data but is not shown conclusively in the point source data. It is not clear how strongly these inconsistencies are related to the deviation from equilibrium of the boundary layer. The Stage II data are much more consistent internally than are the Stage I data, and show trends consistent with fundamental considerations.

Scaling of the Boundary Layer

The difference between the boundary layer developed in the wind tunnel and that found in the atmosphere should be mainly one of scale. The simplest choice for scaling is the momentum boundary layer thickness δ. The δ developed in the atmosphere most frequently ranges from 500 to 1000 m while that found in the wind tunnel is between 7.8 to 9.1 cm, a ratio of 5-to-10 x 10^3.

Another basis for scaling the flow in the wind tunnel to that in the atmosphere is the ratio of gravity to inertia forces, represented by the Froude number, Fr.

$$Fr^2 = U^2/(gL\Delta\rho/\rho)$$

For similarity, the Froude numbers in both the atmosphere and wind tunnel should be made equal. Since the velocity of the atmospheric wind is usually about twice that in the wind tunnel the scaling should be:

$$4(\Delta\rho/\rho L)_{Lab} = (\Delta\rho/\rho L)_{atm}$$

Except for the extreme case of a hot chimney plume, the range of $(\Delta\rho/\rho)_{Lab}/(\Delta\rho/\rho)_{atm}$ is typically 10 to 100. Thus the size ratio L_{atm}/L_{Lab} is typically in the range of 40 to 400. For example, the 0.62 cm injection source would correspond to an atmospheric source of 24.5 to 245 cm.

In a study of this kind, the buoyancy divided by the viscous stress or the Richardson number, Ri, also is significant. Exact modeling requires that the scale of the Richardson numbers in the laboratory and the atomospher e be made the same.

The value of the Richardson number found in atmospheric flows range from 1 to -0.03. Table 2 gives values of the Richardson number and related Monin-Obukhov length scales for all of the laboratory discharge along with those values found in the ambient atmosphere. The laboratory approach Ri = 0, however.

The values of the Richardson number found in the wind tunnel in the discharge region correspond to values that may be found in the atmosphere during conditions of slightly unstable stratification. A comparison of Monin-Obukhov lengths shows that the laboratory values ranged from 0.01 to 10 times the atmospheric values comparing the laboratory discharge to the ambient approach.

It is seen from these scaling calculations that the geometric scaling is not consistent with the other derived length scales. This remains a shortcoming of the simulation and its actual affect on the following comparison of results can not be evaluated here.

Results

The spreading of the buoyant discharge for all of the cases are presented here as plots of isoclines of helium concentrations or as helium concentration maps. Figure 9 shows the isoclines for the Stage I point source. While the applicability of this case to spray canal studies is not straightforward, the figure illustrates an important point. It is seen that initially the spreading in the horizontal direction is faster than in the vertical direction. However, at greater axial distance, the vertical spreading becomes greater than the horizontal spreading. It appears that the effects of the body force term (buoyancy) take some time to be realized while the momentum and

turbulence terms act much more rapidly. The two Stage I cases for a line source with and without roughness are shown in Figures 10 and 11, respectively. Comparison of the two cases shows the appreciable difference in mixing rates due to the added roughness and consequent increase in friction velocity. The delayed effect of the buoyancy is masked by the more gradual spreading in the case without roughness while it is readily apparent in the case with roughness. The first two cases of the Stage II data with the porous plate line source oriented transverse to the flow are shown in Figures 12 and 13. These two figures are helium concentration maps. The small vertical source injection velocity (3 cm/sec) of the helium is seen to have very little affect on the spreading rate since at the end of the porous plate (z = 1.3 cm) the peak concentration is only about 0.4 cm off the floor. The surface roughness again increase the spreading rate considerably and again the buoyancy effects are more clearly visible with surface roughness present. The isoclines for the line source located axially are shown in Figures 14 and 15 for the cases with and without roughness, respectively. As in the previous cases, spreading is more rapid and maximum helium concentrations lower when surface roughness is present. Figure 16 shows helium isoclines 0.6 cm above the floor for the case with the line source located at a 45° angle to the flow. It clearly shows the transverse-line-source-like behavior close to the source and then transition to axial-line-source-like behavior well downstream.

Comparison of Laboratory Data to Models and Field Data

In their study of a point source of diffusion in a neutral shear layer, Rao, et al. [6] define two similarity length scales, one in the vertical direction, η , and one in the horizontal direction, σ, as the distance to the half-maximum concentration. They fit their calculated data found from a Gaussian diffusion model to an exponential equation and the results for both their data and that of Cermak [7] is presented in Table 3. The same exponential equation form was used to fit the data obtained in the present study. These results are also presented in Table 3 for comparison.

It can be seen by comparison of the equations given in Table 3 that the laboratory data exhibits the same type of vertical similarity that is found both using the Gaussian diffusion model and in the atmospheric data and that the exponents found for the y/η term are of the same order of magnitude.

The exponential curve fit of the horizontal spreading data from the diffusion analysis of Rao, et al. [6] and this laboratory study are presented in Table 4.

Again a comparison of the equations shows the same similarity variable type of spreading in the horizontal direction with the exponents of the x/σ term of the same order of magnitude.

A further correlation of the half-maxima as a function of downwind position is presented in Table 5. Comparison of the various correlations shows that the laboratory experimental data show a great similarity to the behavior of both the atmospheric data and the calculated diffusion data. The computed data of Rao, et al. [6] was generated for a point source of diffusion with no buoyancy and included a perturbation in the calculation to simulate roughness. The laboratory data for the point source with roughness show very close agreement for the vertical spreading rates. The calculated data, however, predict a greater rate of spreading in the horizontal direction than the data of this experiment show. This is probably due to the buoyancy of the helium source of this experiment. With the upward directed buoyant fource, there is more material entrained upward and less material spreading in the horizontal direction.

Sutton [8] derived equations for a point source and a line source diffusing into the atmosphere. The equations reduce to the following form for ground level data downwind of a line source or on the centerline downwind of a point source: $C/C_0 = (x/x_0)^n$. Table 6 presents the best fit equations of the form predicted by Sutton as found from this experiment and those found in the field studies by the IIT Waste Energy Management Group from a line source of spray modules in a cooling canal.

A value of n = -1/2 is predicted from theory if the wind velocity and turbulent diffusivity are constant throughout the flow field. The deviation from the predicted value is probably due to the greater shear stress at the ground level and the buoyancy of the discharge.

NUMERICAL MODELLING OF DISPERSION OF HEAT AND HUMIDITY

The spray canal is modelled as a continuously distributed source of heat and moisture. Such a model is a good approximation for dispersion in the near field (over the canal) and is very accurate for far field dispersion. A two dimensional model is considered appropriate for most of the cases except where ambient wind is nearly parallel to the canal. The source strength is proportional to NTU (Number of Transfer Units), flow rates of the sprays and (1-f) where f is the interference allowance which accounts for the heating and humidification of the air. The cooling load of the canal decreases in the windward direction. In the far field (downstream of the canal),

the dissipation of the heat and moisture laden discharge has implications for environmental impact, especially the fogging potential. It is also important in defining the new atmospheric approach conditions for the return leg of the canal.

It is assumed in the analysis that the ambient wind and turbulent diffusivities are not affected by the presence of the spray canal. Attenuation of ambient wind through the sprays is an important factor in computing the local wet bulb temperature and the cooling load. However, in the far field calculations this effect is neglected.

The equation for convective-diffusion in the atmospheric surface layer for enthalpy of the air-vapor mixture per unit mass of dry air is

$$\frac{\partial}{\partial x}(Ui) + \frac{\partial}{\partial z}(Wi) = \frac{\partial}{\partial z}(K_i \frac{\partial i}{\partial z}) + (Q_s''' + \dot{m}_e''' i_g)/\rho_a \qquad (1)$$

Where K_i is the vertical turbulent diffusivity for i, Q_s''' is volumetric sensible heating rate, $\dot{m}_e'''$ is volumetric mass evaporation rate, i is the saturated liquid water specific enthalpy and ρ_a is dry-air density. Similarly, for vapor moisture transport characterized by the humidity (mass of vapor per unit mass of dry air)

$$\frac{\partial}{\partial x}(Uw) + \frac{\partial}{\partial z}(Ww) = \frac{\partial}{\partial z}(K_w \frac{\partial w}{\partial z}) + \dot{m}_e''' / \rho_a \qquad (2)$$

Assuming unit turbulent Schmidt number [10,14] and $K_i = K_w = K$, Equations (1) and (2) may be combined to that of the total heat, $h = i - wi_f$, which turns out to be a function only of the wet bulb temperature (WBT). A thermodynamic property

$b = \frac{dh}{dT_{WB}}$ [13-14] is evaluated at the average between T and T_{WB} and is denoted b_f for the purpose of formulating the relation of h to T_{WB}. The resulting equation for T_{WB} may be simplified by using the continuity equation which yields

$$U\frac{\partial T_{WB}}{\partial x} + W\frac{\partial T_{WB}}{\partial z} = \frac{\partial}{\partial z}(K\frac{\partial T_{WB}}{\partial z}) + (Q_s''' + \dot{m}_e''' i_{fg})/\rho_a b_f \qquad (2b)$$

The source term on the RHS contains the rate of evaporative cooling of the spray per unit volume. In the spray region I (only)

$$Q_s''' + \dot{m}_e'''' \, i_{fg} = - C_w \, \Delta T_s \, \dot{m}_s''' / z_s$$

where $-\Delta T_s$ is the spray cooling range and i_{fg} is the latent heat of water. Z_s is the averaged spray height and $\dot{m}_s''$ is the mass flow rate per unit collection area. The cooling range is given by the NTU model (NTU $\approx$ ntu) wherein [10,13,14]

$$- \Delta T_s = (T - T_{WB})\left(1 - e^{-ntu \frac{b_f}{C_w}}\right)$$

$$U \frac{\partial T_{WB}}{\partial x} + W \frac{\partial T_{WB}}{\partial z} = \frac{\partial}{\partial z}\left(K \frac{\partial T_{WB}}{\partial z}\right) + \frac{C_w}{b_f} \frac{1}{\rho_a} \frac{\dot{m}_s''}{Z_s}\left(1 - e^{-ntu \frac{b_f}{C_w}}\right) \cdot (T - T_{WB})$$

Non dimensionalizing the above equation we get,

$$\bar{U} \frac{\partial f}{\partial \bar{x}} + \bar{W} \frac{\partial f}{\partial \bar{z}} = \frac{\partial}{\partial \bar{z}}\left(\bar{K} \frac{\partial f}{\partial \bar{z}}\right) + H(1 - f)$$

where $\bar{U}, \bar{W} = \frac{U}{U_{2m}}, \frac{W}{U_{2m}}$

U_{2m} = velocity at 2 meter height

$\bar{K} = \frac{K}{U_{2m} L}$

$\bar{x}, \bar{z} = x/L, z/L$

$$H = \frac{C_w}{b_f} \frac{1}{\rho_a} \frac{L}{z_s} \dot{m}_s''' \left(1 - e^{-ntu \frac{b_f}{C_w}}\right) \frac{1}{U_{2m}}$$

and $f = \frac{T_{WB} - T_{WB\infty}}{T - T_{WB\infty}}$

Where T_{WB} and $T_{WB\infty}$ are the local and ambient wet bulb temperatures respectively and T is the canal temperature.

The velocity in the surface layer is taken to be

$$U = \frac{\kappa U_*}{(1-\beta)} \left[\left(\frac{z}{z_o}\right)^{1-\beta} - 1\right]$$

$$W = 0$$

and the turbulent transport diffusivity is taken as

$$K = \kappa U_* z_o \left(\frac{z}{z_o}\right)^{\beta}$$

Where κ is Karman's constant (0.40), U_* is the frictional velocity, z_o is the approach surface roughness, and is the stability parameter.

$\beta > 1.0$ unstable atmosphere

$\beta \geq 1.0$ neutral atmosphere

$\beta < 1.0$ stable atmosphere

Boundary conditions are:

$f = 0$ at $\bar{x} = 0$ (spray canal leading edge)

$f = 0$ as $\bar{z} \to \infty$ $(\bar{x} \geq 0)$

$\frac{\partial f}{\partial \bar{z}} = 0$ $\bar{z} = 0$ $(\bar{x} \geq 0)$

An insulated boundary condition is appropriate over the canal surface and the ground downstream of the canal. The canal surface contributes very little.

Numerical Solution Results

The governing equation is parabolic and is solved by Keller's box algorithm (for details see [15]). Computation is started at $\bar{x} = 0$ where the f profile is specified and marching proceeds in the downwind direction. At the end of the canal the interference allowance is obtained. From then onwards, the calculations are continued without the source term. Numerical results are obtained for conditions identical to field observation. Figure (17) illustrates the vertical spread of the spray canal discharge for various values of β. The boundary of the discharge is obtained by the criterion that the value of f becomes 0.001 at the boundary. For unstable conditions the discharge spreads to greater heights than for neutral or stable cases. Furthermore, the discharge grows linearly. Figure (18) shows the decay of ground level interference allowance. The decay is

most rapid for the most unstable case and least for the most stable case. The field data falls below the $\beta = 1.2$ line. The data was taken on a hot summer afternoon (value of β perhaps equal to 1.2). However, the value of β under the field condition was not recorded, and hence, an accurate comparison is not possible. The field data are also likely to decay more rapidly due to the buoyancy effect and are likely to over predict the values of f. Fogging potential is highest in winter conditions (highest potential $(T - T_{WB\infty})$ and in the early morning hours (most stable atmosphere) and is least in summer (lowest value of $(T - T_{WB\infty})$ and in afternoon hours (most unstable atmosphere).

By extrapolating the plume boundary line the location of a virtual line source upstream of the spray canal can be determined. The location of the virtual source depends on the stability of the atmosphere. For the unstable cases the virtual source lies close to the origin of the canal and moves upstream as the value of β decreases. This virtual source produces the same amount of heat and humidity as the entire spray canal (the finite source). Such a virtual source does not reproduce the f profile over the source but reproduces the f profile downstream of the canal. Such virtual sources were used by Arndt and Barry [16] in a computer model to predict both heating and mumidification within the distributed source as well as the environmental effects downwind.

DISCUSSION OF RESULTS

The three component parts of this investigation yield results which are in only partial agreement. The field experiments show a ground-level fall off of wet-and dry-bulb temperature with distance to the -3/2 power. The laboratory line-source data show an exponent of roughly -1/2 to -3/4 and indicate a dependence of this parameter on surface roughness. However, the limited amount of data do not clearly show the nature of this dependence. The analytical study gives results of about -1/2 to -1 for the exponent for various values of the atmospheric stability parameter which are in good agreement with the laboratory studies.

The envelope of the discharge downstream of the canal appeared to grow in height as the first power of downstream distance upon field observation during fogging conditions. The analysis indicates a growth proportional to distance raised to a power less than one for various values of the stability parameter. Combination of the spreading rate equations derived from the laboratory data agree with the analytical results and show an exponent of approximately 0.6 for a representative line-source case. The disagreement between the three sets of results is

in part due to the fact that the laboratory study treated a buoyant discharge. The analytical study treated a non-buoyant discharge for several atmospheric stability cases and the field study was on a buoyant discharge. The wide variations in atmospheric conditions make it very difficult to mock up actual canal behavior in the laboratory or in an analysis. However, the good agreement between analysis and laboratory simulation indicates that more complete simulation studies of canal behavior are worthwhile and that the response of canal behavior to various changes in parameters can be studied with these models.

The laboratory study and the analytical model did not treat the possibility of fogging. Yet fogging is an important environmental consideration with spray canals. A first approximation to fogging potential in a given case can be obtained from concentration maps assuming a relationship between the heat and mass transfer. The result from such an analysis indicating fogging is possible at a certain downstream distance implies that concentrations from that point on are in error but does not insure that fogging will in fact take place.

REFERENCES

1. Papamarcos, J., "Spinning Discs: A Better Way to Cool Pond Water," Power Engineering, 75, 9, 54-57, Sept. 1971

2. Stewart, R. and Nelson, R. T., "Weather Modification due to Spray Pond Cooling," ASME Paper 75-HT-1, August 1975.

3. Guyer, E. C. and Golay, M. W., "A Model for Salt Drift Deposition from Spray Ponds," I AEA-SM-187/37, International Atomic Energy Agency, Vienna, 1975.

4. Schrecker, G. O., and Henderson, G. D., "Salt Water Condenser Cooling: Measurements of Salt Water Drift from a Mechanical Draft Wet Cooling Tower and Spray Modules and Operating Experience with Cooling Tower Materials," Proceedings of American Power Conference, Vol. 38, 1976 (in press).

5. Cermak, J. E., "Applications of Fluid Mechanics to Wind Engineering--A Freeman Scholar Lecture, J. Fluids Eng., 9, 38, 1975.

6. Rao, K. S., Nee, V. W., and Yang, K. T., "Mass Diffusion from a Point Source in a Neutral Turbulent Shear Layer," ASME Paper 74-HT-43, 1974.

7. Cermak, J. E., "Lagrangian Similarity Hypothesis Applied to Diffusion in Turbulent Shear Flow," J. Fluid Mech., 15, 49-64, 1963.

8. Sutton, O. G., Micrometeorology, McGraw Hill, N.Y., 1953.

9. Nagib, H. M., Morkovin, M. V., Yung, J. T., and Tan-Atichat, J., "On Modelling of Atmospheric Surface Layers by the Counter-Jet Technique," AIAA J., 14, 18-190, 1976.

10. Porter, R. W., Yang, U. M. and Yanik, A., "Thermal Performance of Spray Cooling Systems," Proceedings of American Power Conference, Vol. 38, 1458-1472, 1976.

11. Chaturvedi, S. and Porter, R. W., "Effect of Air-Vapor Dynamics on Interference Allowance for Spray Cooling Systems," IIT Waste Energy Management Report TR-77-1, March 1977.

12. Porter, R. W. and Chen, K. H., "Heat and Mass Transfer of Spray Canals," Journal of Heat Transfer, Vol. 96, 3, 286-291, August 1974.

13. Porter, R. W., "Analytical Solution for Spray-Canal Heat and Mass Transfer," Joint ASME Paper 74-HT-58, AIAA Paper 74-764, July 1974.

14. Yang, U. M. and Porter, R. W., "Thermal Performance of Spray Cooling Systems-Theoretical and Experimental Aspects," IIT Waste Energy Management Report TR-76-1, December 1976.

15. Keller, H. B., "A New Difference Scheme for Parabolic Problems," Numerical Solutions of Partial Differential Equations, II, J. Bramble (ed.) Academic Press, New York, 1970. pp [265,293]

16. Arndt, C.R., and Barry, R.E., "Simulation of Spray Canal Cooling for Power Plants--Performance and Environmental Effects," ASME paper 76-HT-28,1976.

TABLE 1

Comparison of Boundary Layer Parameters for Stage I and Stage II Studies

		Stage I				Stage II	
		Point Source		Line Source		(all)	
		W/0*	W**	W/0	W	W/0	W
Friction velocity squared	U_*^2	0.15	0.15	0.14	0.38	0.080	0.40
Boundary layer thickness	δ	3-1/16"	3-9/16"	3-1/6"	3-9/16"	3"	4"
Free stream velocity	U	11 ft/sec				9 ft/sec	
Free stream turbulence intensity	u'_{fs}	0.85%				~1%	
Velocity profile exponent	n	4	3	7	4	5-6	4
Ratio of transverse to axial turbulence intensities	$\sqrt{v'^2/u'^2}$	0.67-0.69		0.67-0.74		0.74-0.78	
Turbulence microscale (ft)	λ	1.95×10^{-4}	1.51×10^{-2}			$.69\times10^{-2}$	2.87×10^{-2}
Turbulence macroscale (ft)	Λ	3.14×10^{-2}	5.14×10^{-2}			2.87×10^{-2}	3.9×10^{-2}

* W/0 refers to without roughness

** W refers to with roughness

TABLE 2

Richardson Numbers and Monin-Obukhov Length Scales for Laboratory and Atmospheric Flows

Case	R_i	L(m)
1) Stage I point source without roughness(W/0)	-6.58×10^{-4}	-1.21
2) Stage I point source with roughness(W)	-57×10^{-4}	-13.8
3) Stage I line source(W/0)	-3.17×10^{-4}	-2.51
4) Stage I line source (W)	-1.14×10^{-4}	-6.95
5) Stage II Transverse source (W/0)	0.386×10^{-4}	-276
6) Stage II Transverse source (W)	-0.293×10^{-4}	-102
7) Stage II Axial source (W/0)	-2.34×10^{-4}	-48
8) Stage II Axial source (W)	-1.21×10^{-4}	-206
9) Pasquill[18] O'Neill data	~0.028	-62 to -250
10) Webb [19], O'Neill data	~0.014	-98 to -146

TABLE 3

Exponential Equation Fit of Spreading in the Vertical Direction for the Experimental Data and for Theoretical Point Source Data

Equation	Source of Data
$C/C_{max} = \exp[\ 0.693(z/\eta)^{1.8}]$	Rao, Nee and Yang [6]
$C/C_{max} = \exp[-0.693(z/\eta)^{1.4}]$	Cermak [7]
$C/C_{max} = \exp[-0.693(z/\eta)^{1.96}]$	Stage I data for a point source Without Roughness.
$C/C_{max} = \exp[-0.693(z/\eta)^{1.89}]$	Stage I data for a point source with roughness.
$C/C_{max} = \exp[-0.693(z/\eta)^{1.93}]$	Stage I data for a line source without roughness.
$C/C_{max} = \exp[-0.693(z/\eta)^{1.71}]$	Stage I data for a line source with roughness.
$C/C_{max} = \exp[-0.693(z/\eta)^{2.50}]$	Stage II data for a transverse line source without roughness.
$C/C_{max} = \exp[-0.693(z/\eta)^{1.66}]$	Stage II data for a transverse line source with roughness.
$C/C_{max} = \exp[-0.693(z/\eta)^{2.00}]$	Stage II data for a axial line source without roughness.
$C/C_{max} = \exp[-0.693(z/\eta)^{2.14}]$	Stage II data for a axial line source with roughness.

TABLE 4

Exponential Equation Fit of Spreading in Horizontal Direction for Point Source Experimental and Theoretical Data

Equation	Source of Data
$C/C_{max} = \exp[-0.693(y/\sigma)^{2}]$	Rao, et al [6]
$C/C_{max} = \exp[-0.693(y/\sigma)^{2.05}]$	Stage I Point Source Without Roughness
$C/C_{max} = \exp[-0.693(y/\sigma)^{1.62}]$	Stage I Point Source With Roughness
$C/C_{max} = \exp[-0.693(y/\sigma)^{1.99}]$	Stage II Axial Line Source Without Roughness
$C/C_{max} = \exp[-0.693(y/\sigma)^{2.09}]$	Stage II Axial Line Source With Roughness

TABLE 5

Similarity Variables from Exponential Spreading Equations as a Function of Downstream Distance (η,σ in cm; x in ft)

Equation	Source of Data
$\eta = 0.121(x)^{0.69}$	Rao, Nee, and Yang [6]
$\eta = \text{const}(x)^{0.71}$	Cermak [7]
$\eta = 0.113(x)^{0.590}$	Stage I Point Source w/o Roughness
$\eta = 0.154(x)^{0.706}$	Stage I Point Source with Roughness
$\eta = 0.274(x)^{0.410}$	Stage I Line Source w/o Roughness
$\eta = 0.246(x)^{0.327}$	Stage II Line Source w/o Roughness
$\eta = 0.238(x)^{0.597}$	Stage II Transverse Line Source with Roughness
$\eta = 0.324(x)^{0.278}$	Stage II Axial Line Source w/o Roughness
$\eta = 0.136(x)^{0.754}$	Stage II Axial Line Source with Roughness
$\sigma = 0.223(x)^{0.61}$	Rao, Nee, and Yang [6]
$\sigma = \text{const}(x)^{0.60}$	Cermak [7]
$\sigma = 0.15(x)^{0.54}$	Stage I Point Source w/o Roughness
$\sigma = 0.22(x)^{0.53}$	Stage I Point Source with Roughness
$\sigma = 0.208(x)^{0.380}$	Stage II Axial Line Source w/o Roughness
$\sigma = 0.190(x)^{0.596}$	Stage II Axial Line Source with Roughness

TABLE 6

Power Law Fit of Experimental Data of Ground Concentrations Downwind of a Source

Equation	Source of Data
$C/C_o = (x/x_o)^{-0.769}$	Stage II Transverse Line Source Without Roughness
$C/C_o = (x/x_o)^{-0.556}$	Stage II Transverse Line Source With Roughness
$C/C_o = (x/x_o)^{-1.22}$	Stage II Axial Line Source Without Roughness
$C/C_o = (x/x_o)^{-1.21}$	Stage II Axial Line Source With Roughness
$C/C_o = 0.97(x/x_o)^{-1.20}$	Stage I Point Source Without Roughness
$C/C_o = 0.98(x/x_o)^{-0.33}$	Stage I Point Source With Roughness
$C/C_o = (x/x_o)^{-0.43}$	Stage I Line Source Without Roughness
$C/C_o = 0.96(x/x_o)^{-0.78}$	Stage I Line Source With Roughness
$C/C_o = (x/x_o)^{-3/2}$	Field Study

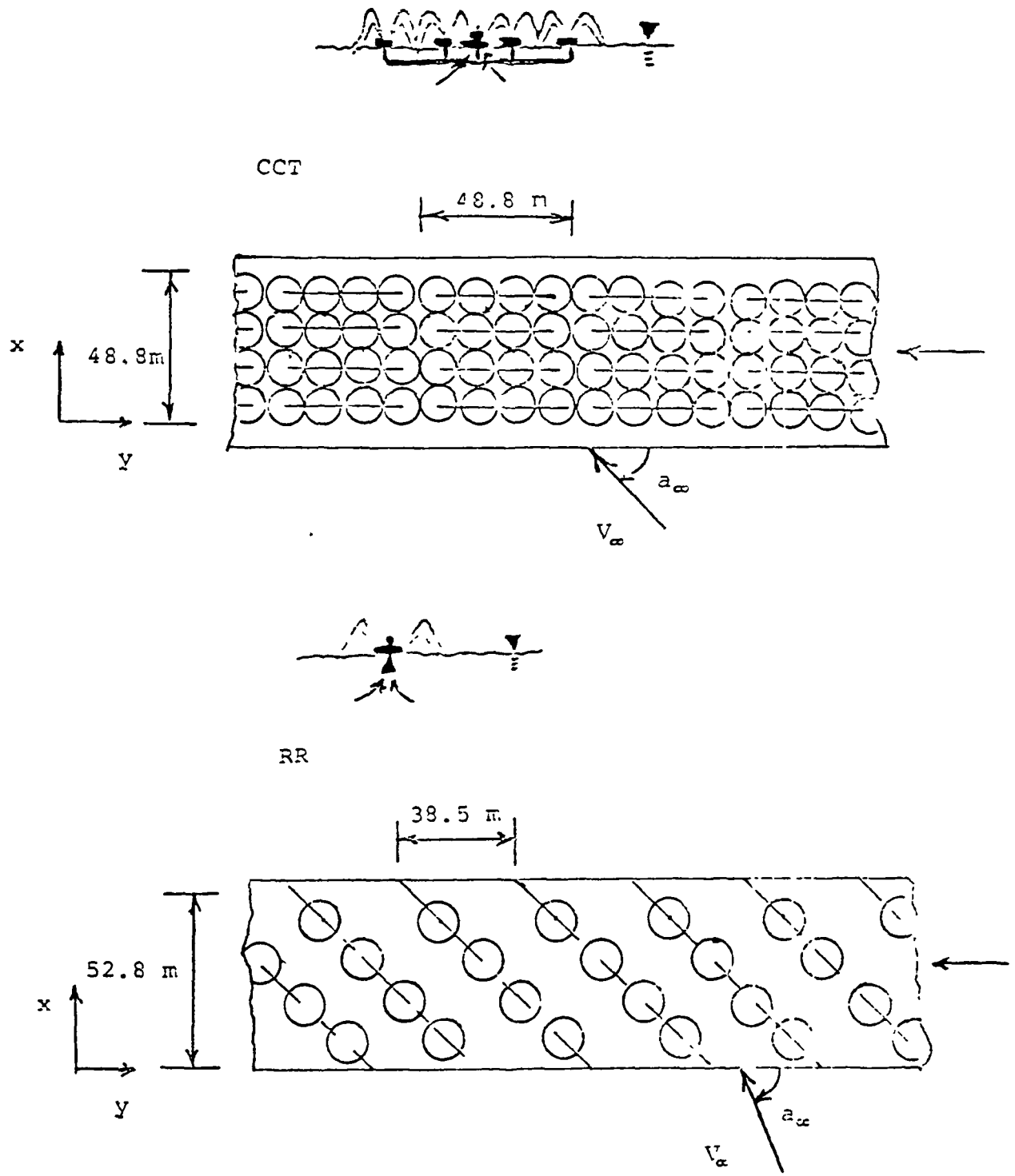

Figure 1. Layout of Sprays at Quad-Cities Station.

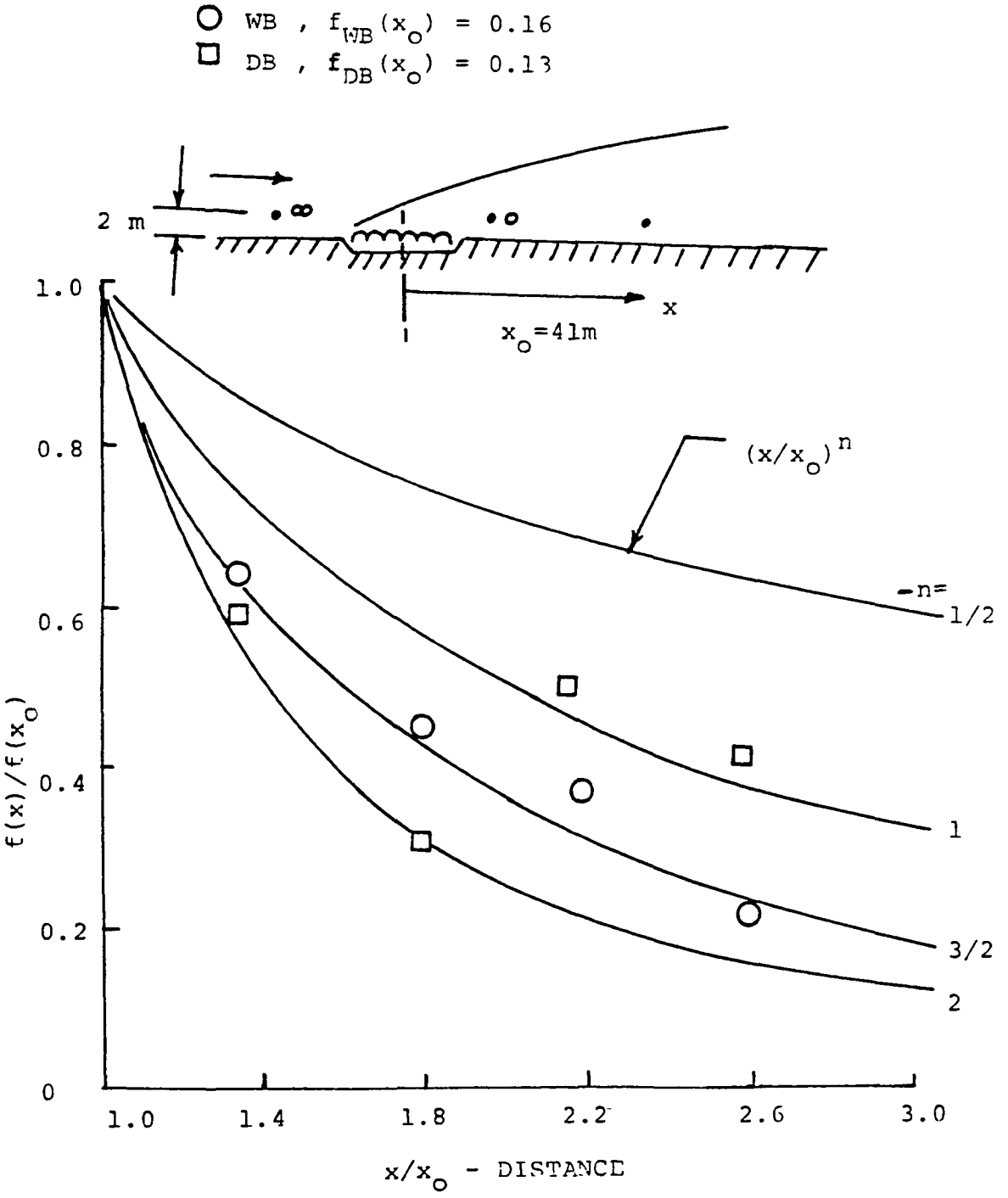

Figure 2. Field Experimental Data from Quad-Cities Station.

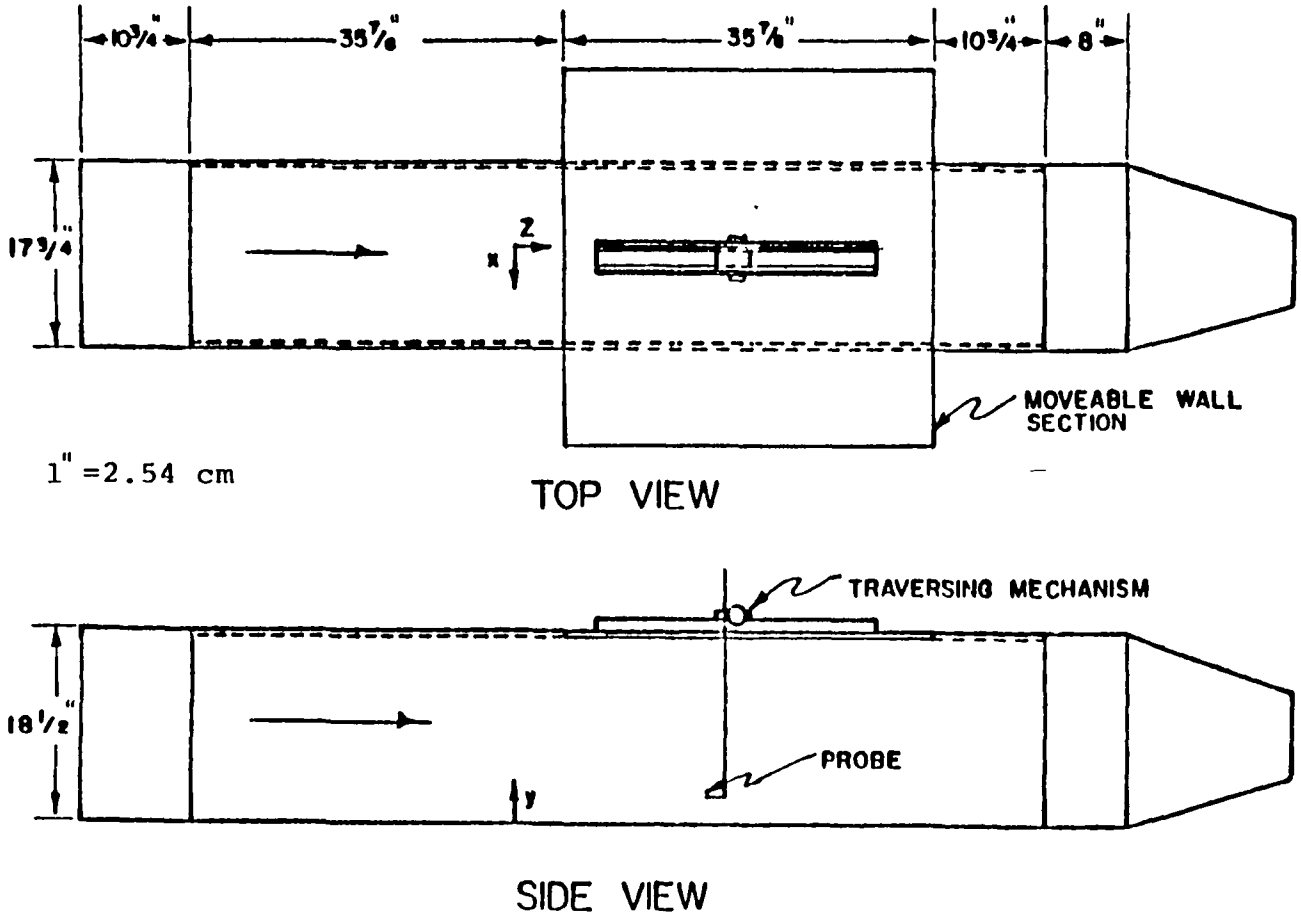

Figure 3. Experimental Wind Tunnel.

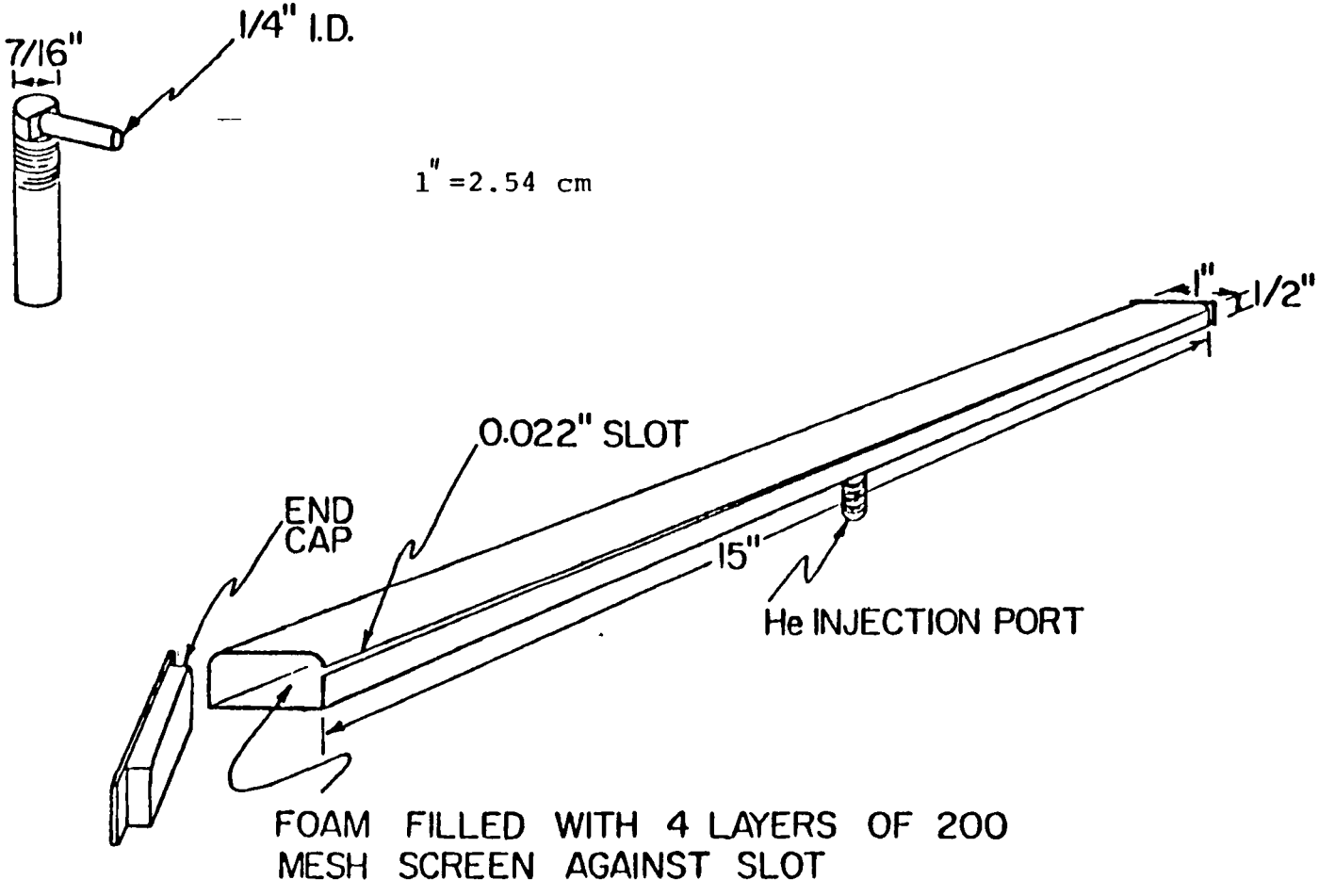

Figure 4a. Injection Devices, Stage I.

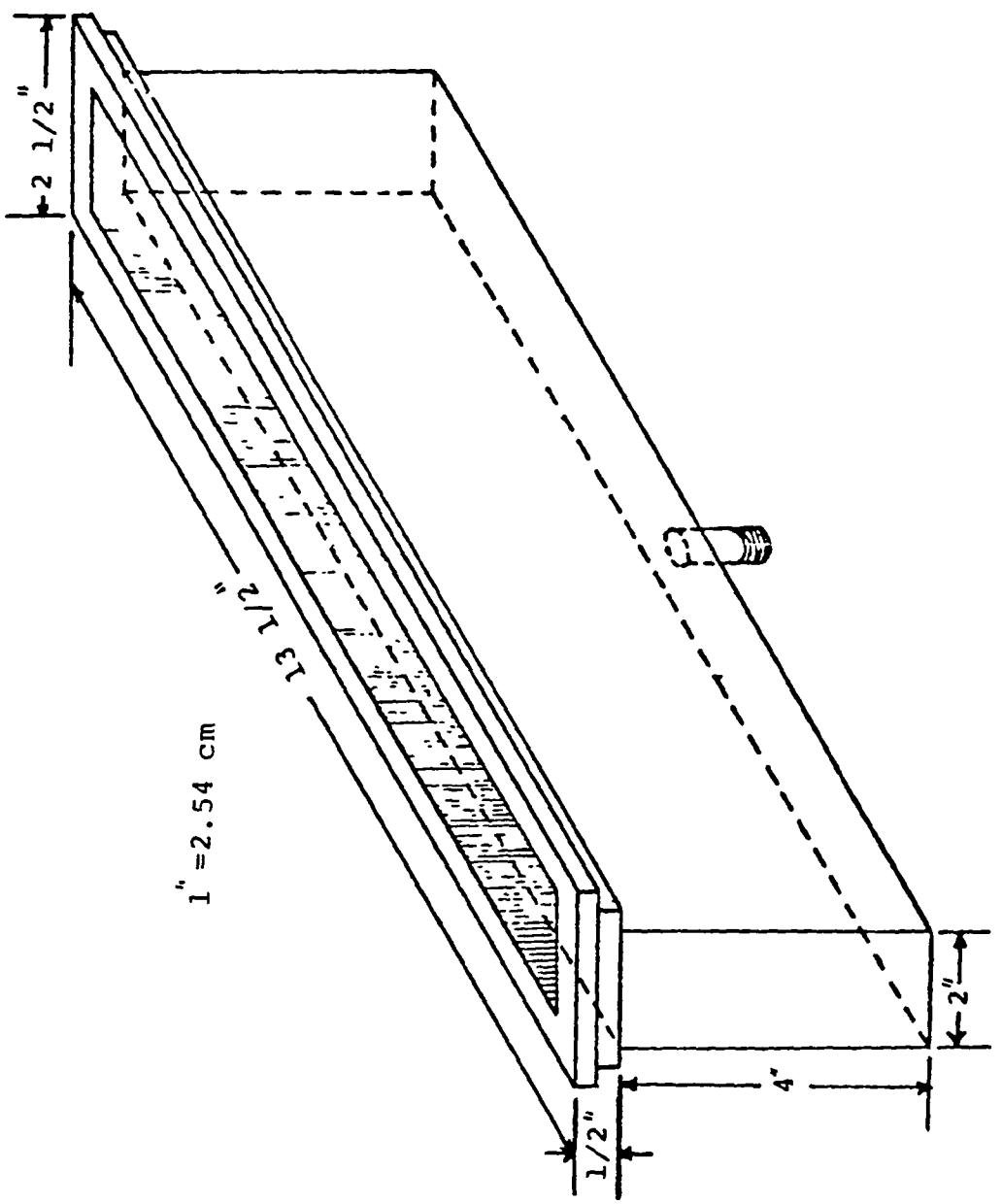

Figure 4b. Injection Device, Stage II.

HW

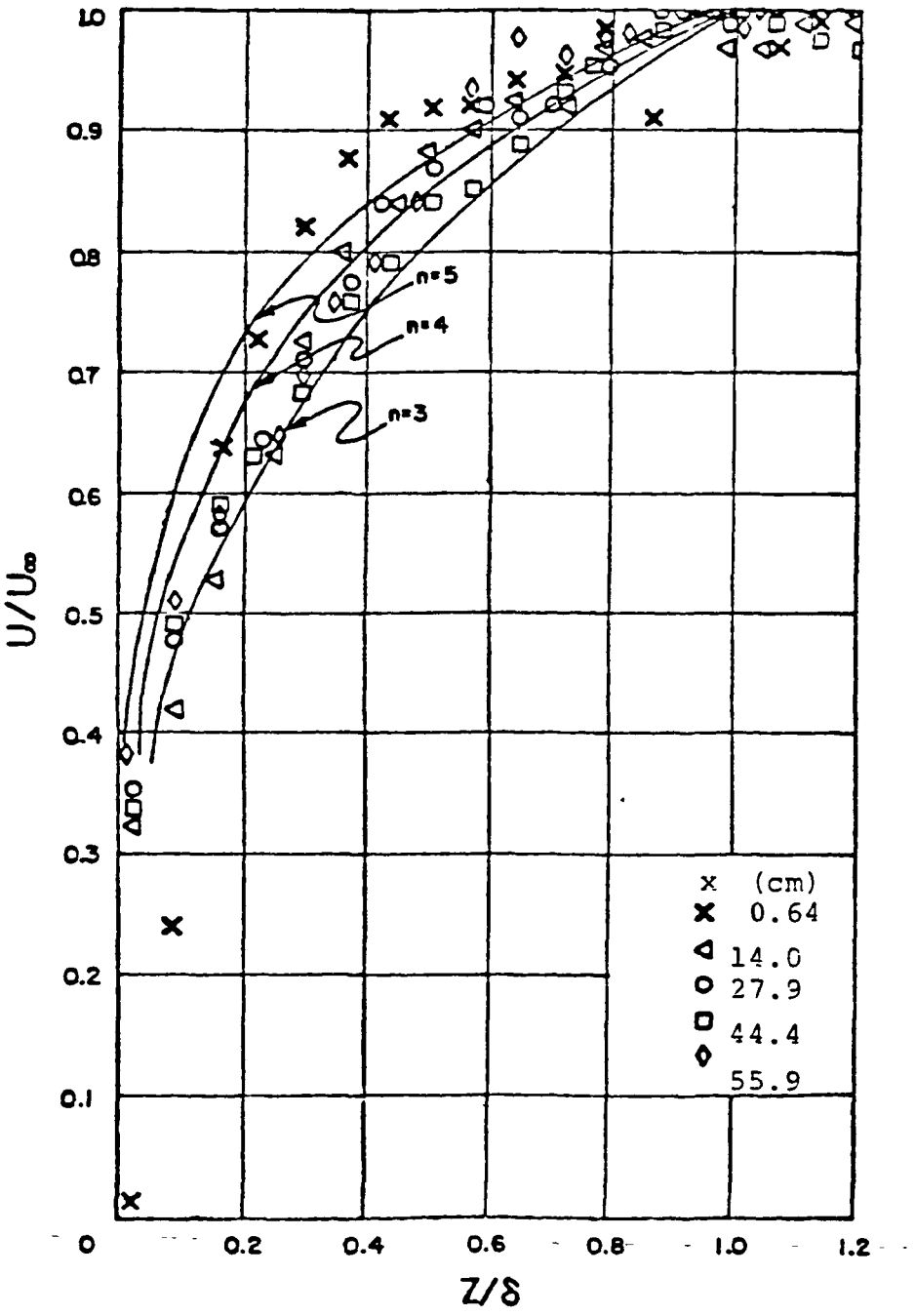

Figure 5. Velocity Profile for a Line Source with Roughness, Stage I.

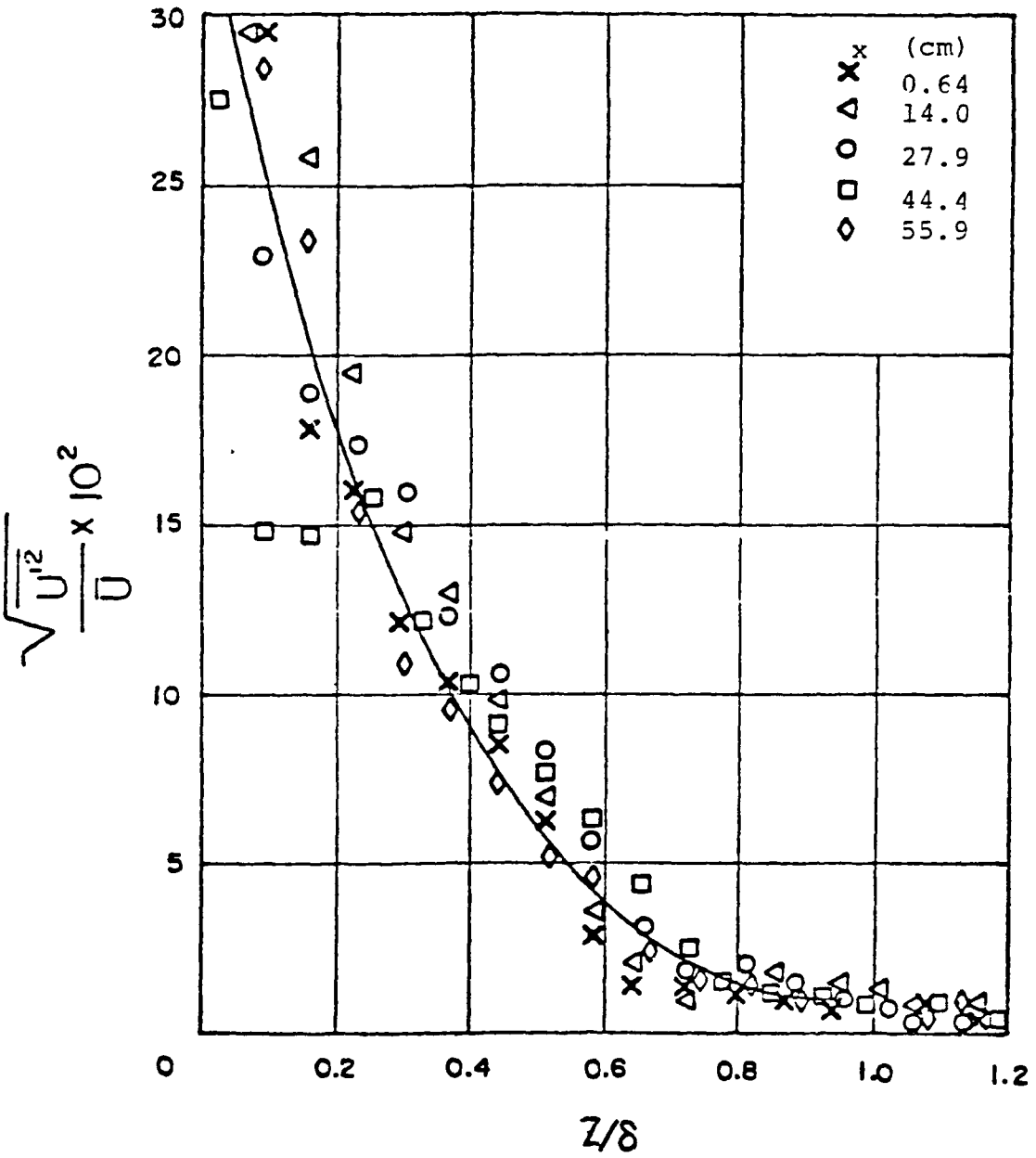

Figure 6. Axial Turbulence Intensity Profile for a Line Source with Roughness, Stage I.

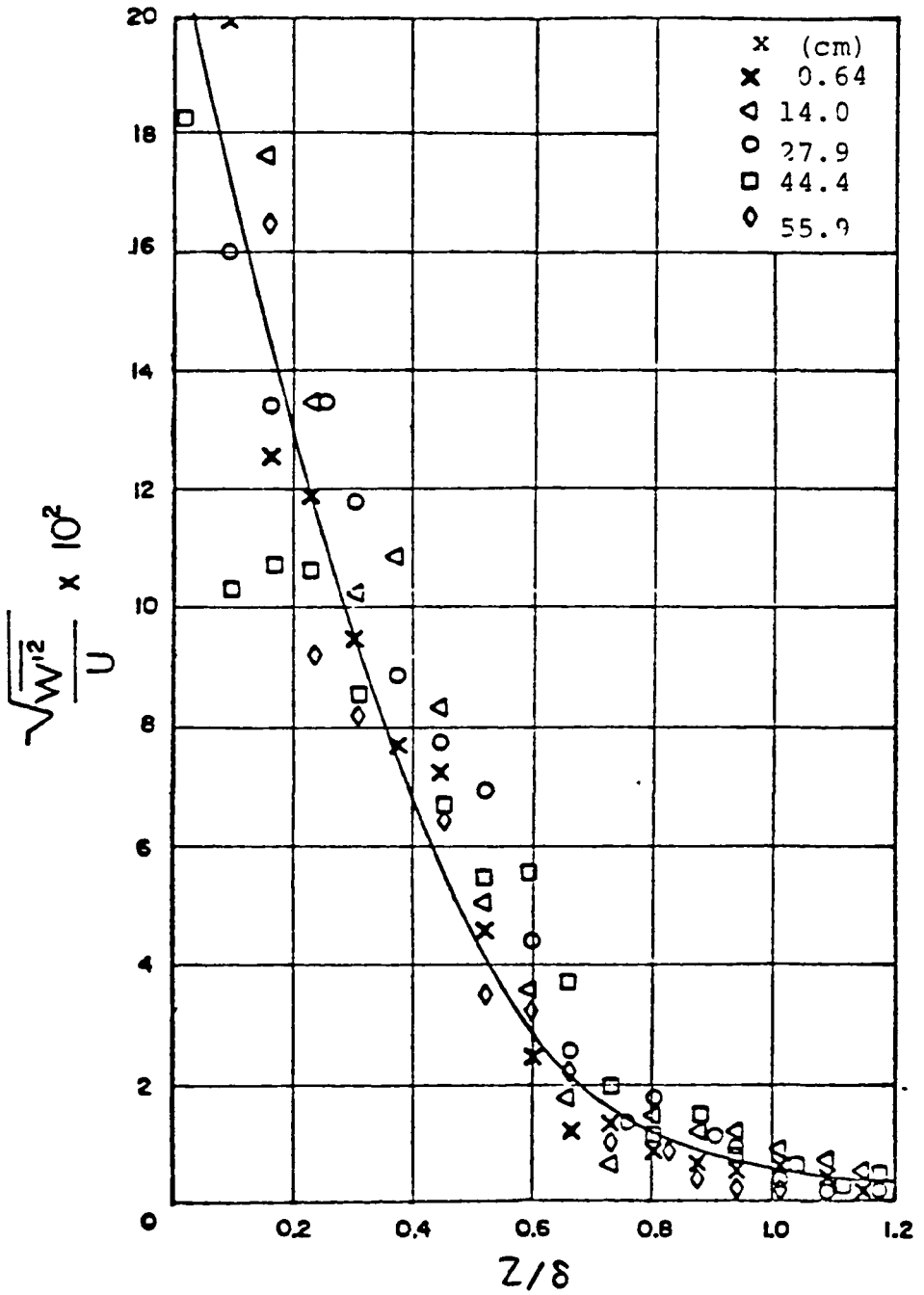

Figure 7. Transverse Turbulence Intensity Profile for a Line Source with Roughness, Stage I.

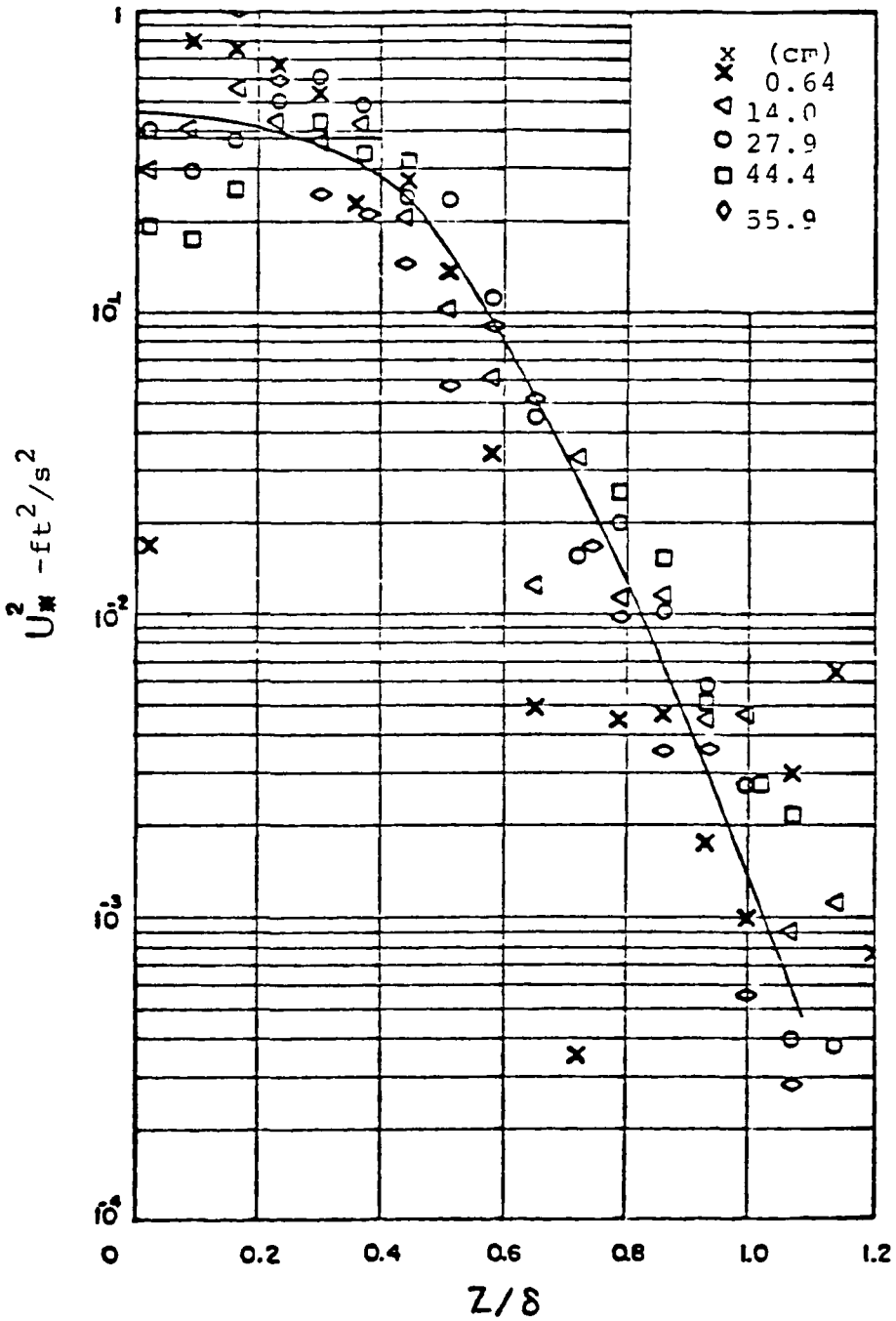

Figure 8. Reynolds Stress for a Line Source with Roughness, Stage I.

HW

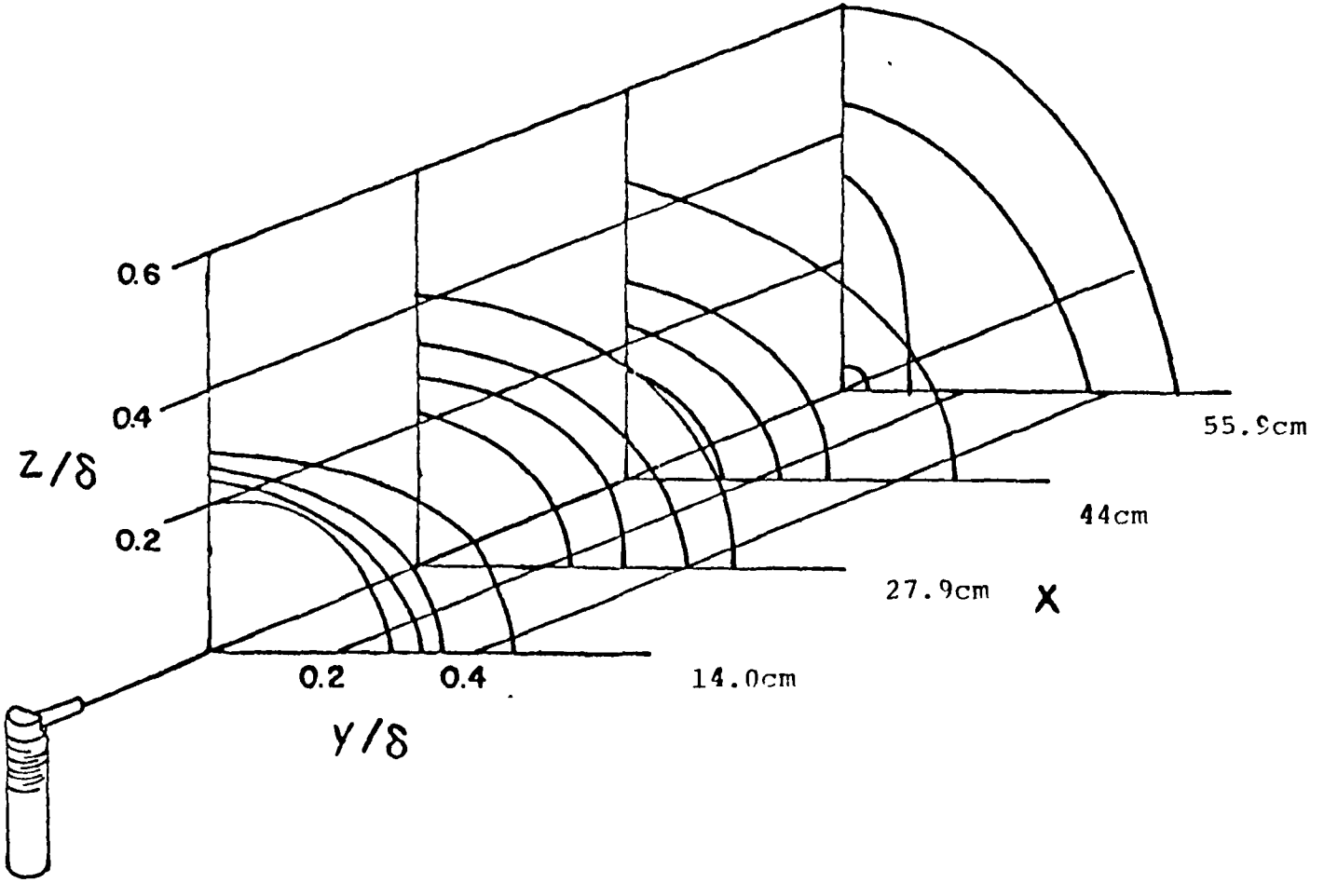

Figure 9. Helium Concentration Isoclines for a Point Source with Roughness 0.25%, 0.50%, 0.75% and 1.00%.

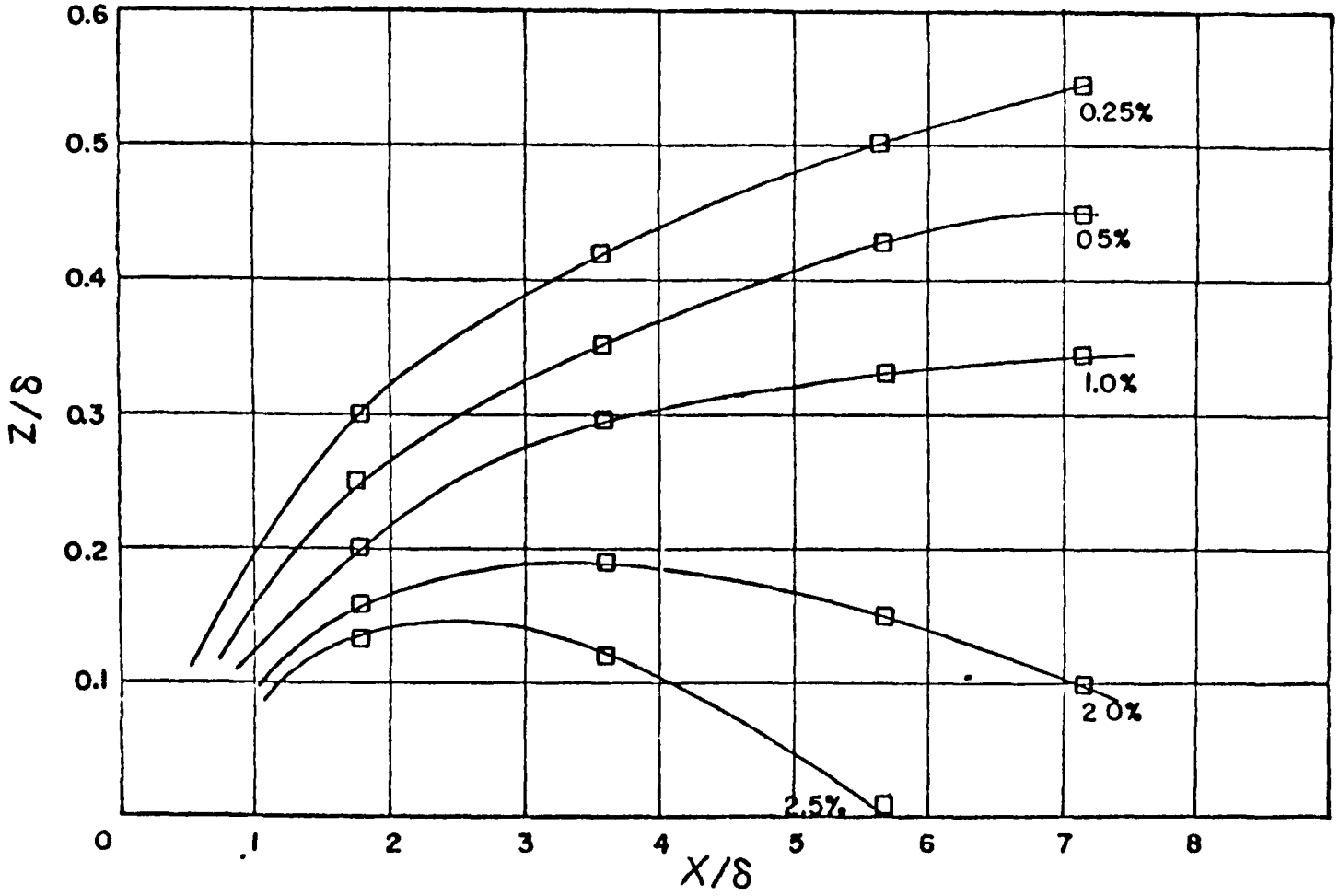

Figure 10. Lines of Isoconcentration for a Line Source Without Roughness, Stage I.

HM

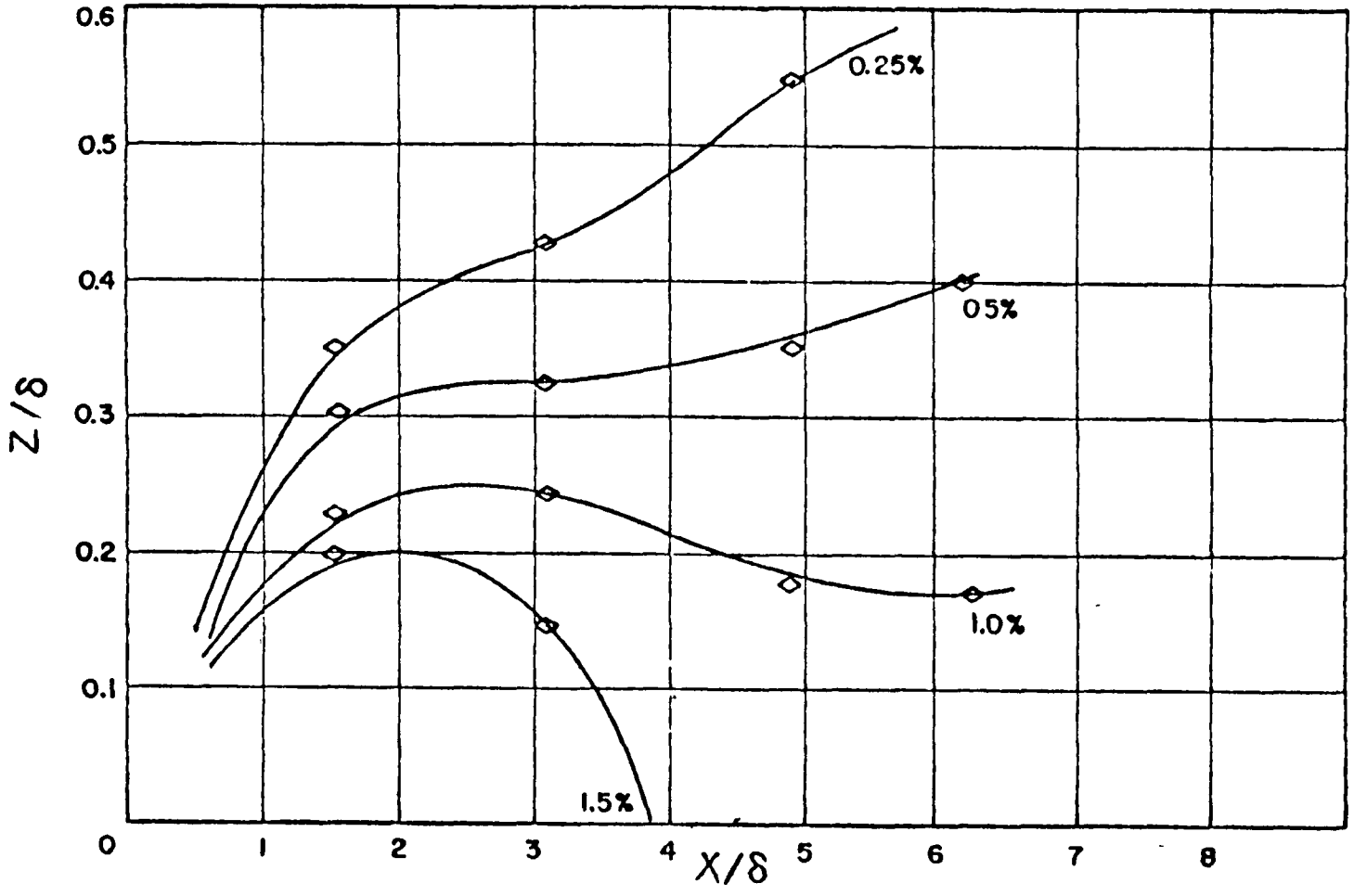

Figure 11. Lines of Isoconcentration for a Line Source with Roughness, Stage I.

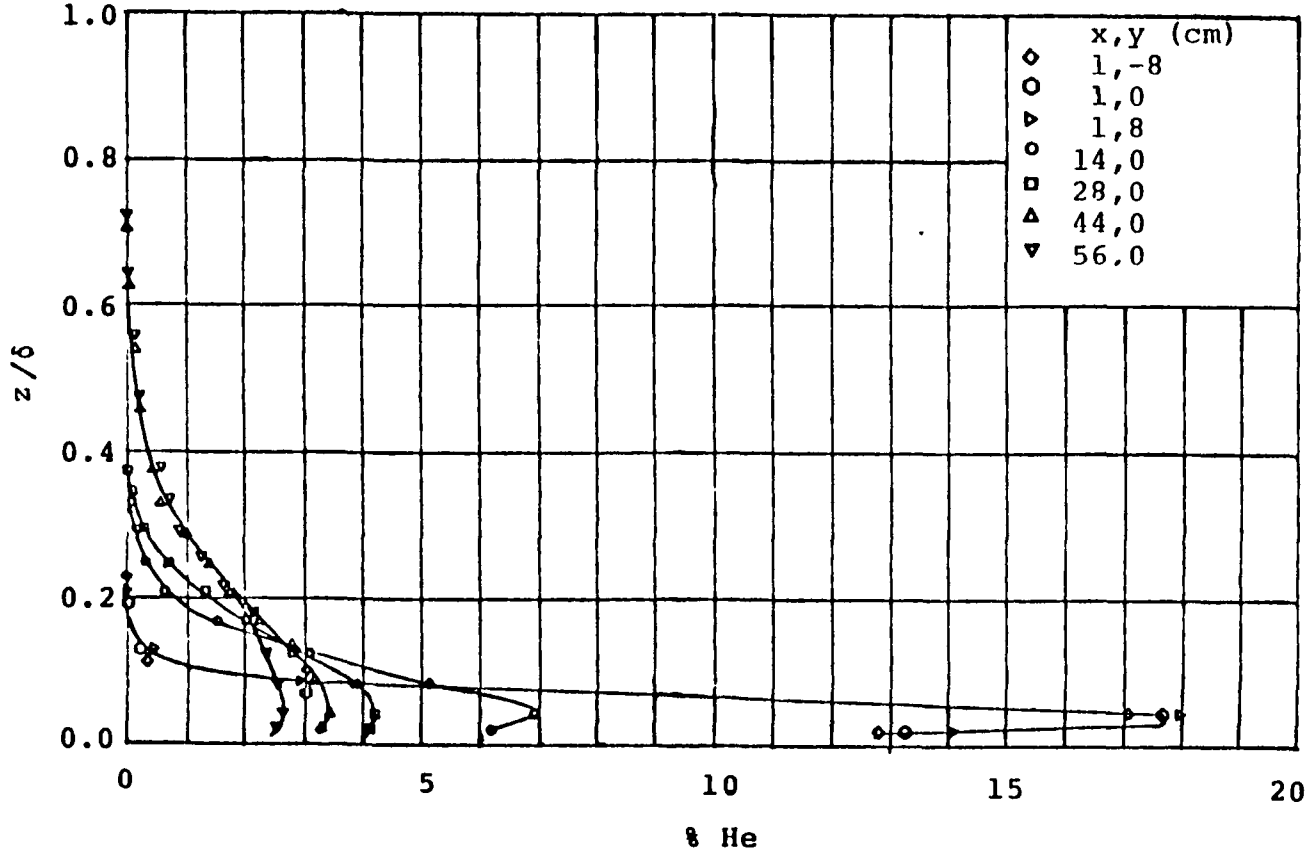

Figure 12. Helium Concentration Profiles for Transverse Line Source Without Roughness, Stage II.

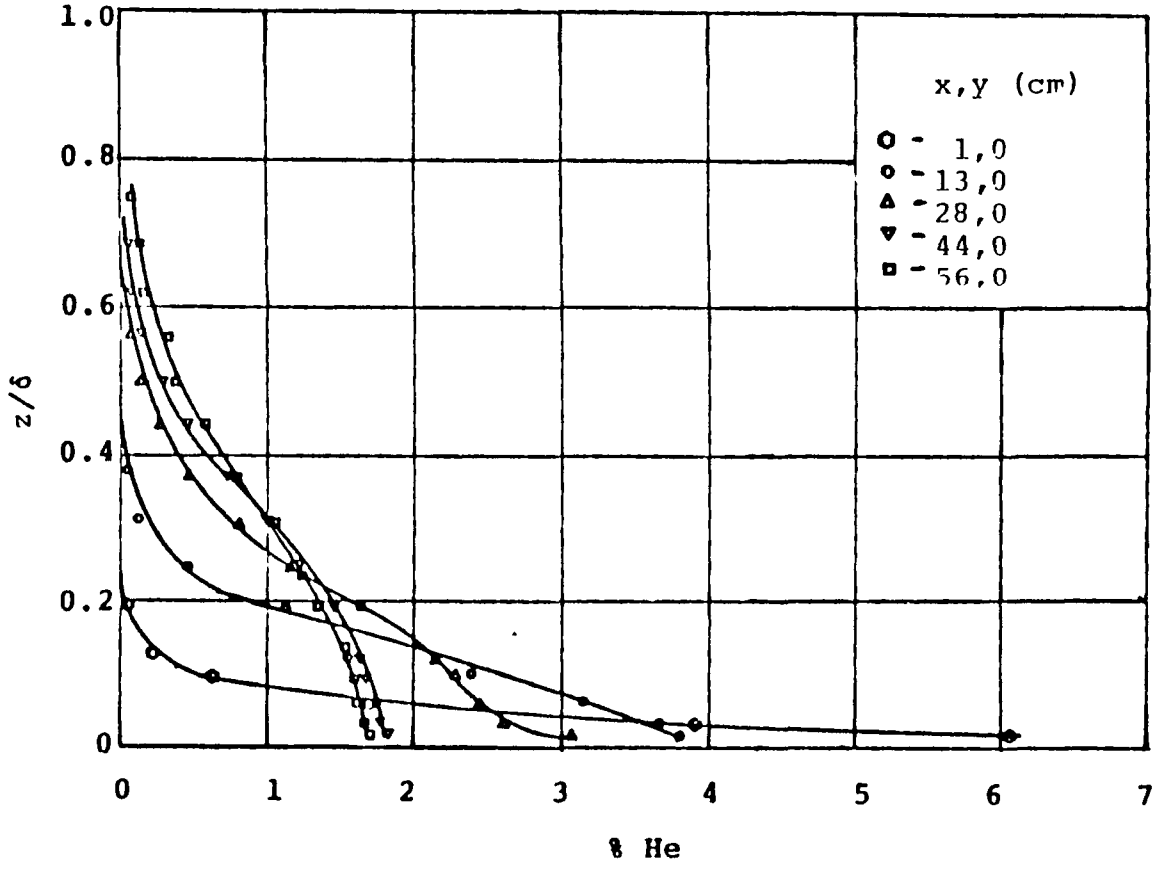

Figure 13. Helium Concentration Profiles for Transverse Line Source with Roughness, Stage II.

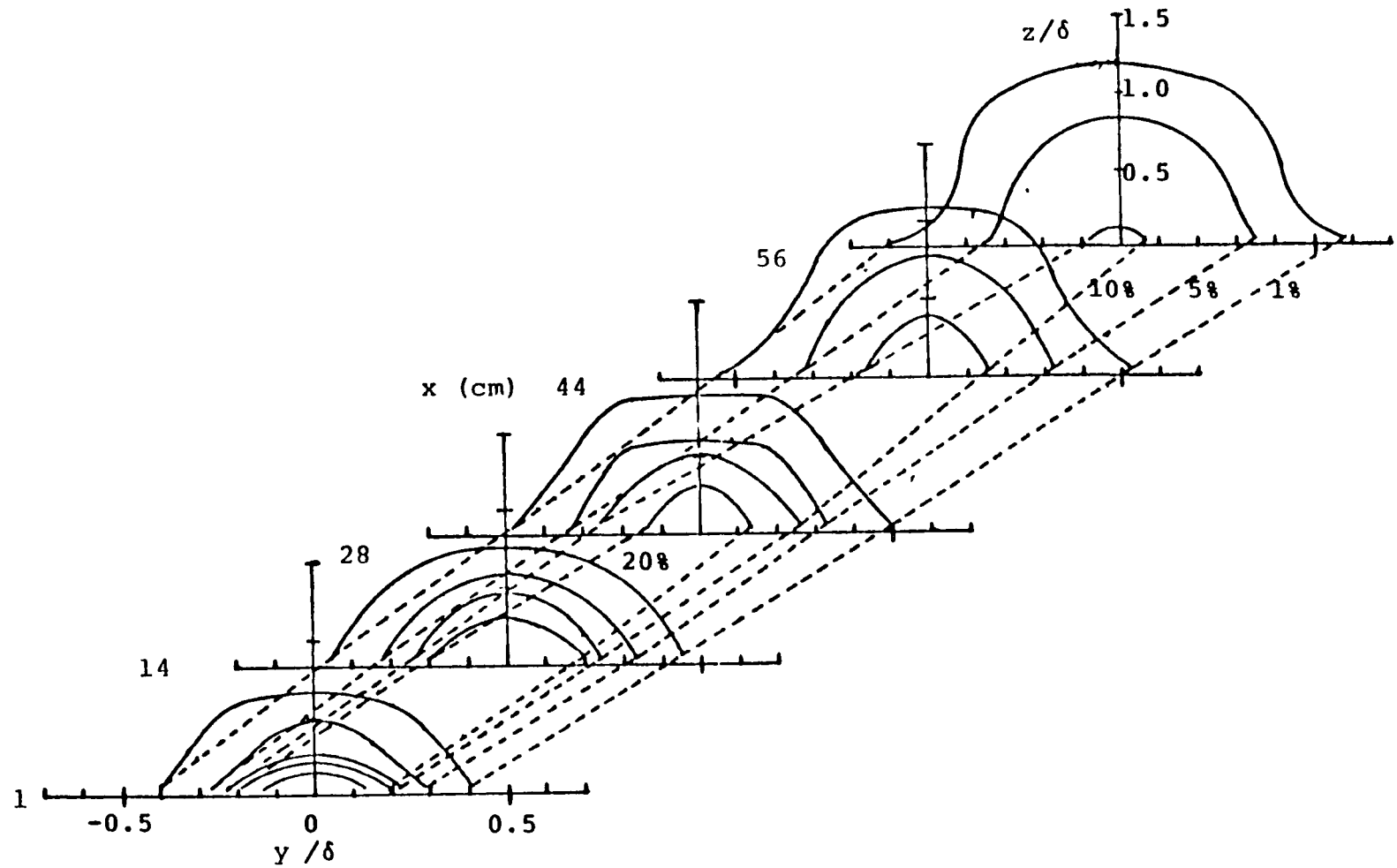

MH Figure 14. Helium Concentration Isoclines for Axial Line Source Without Roughness Stage II.

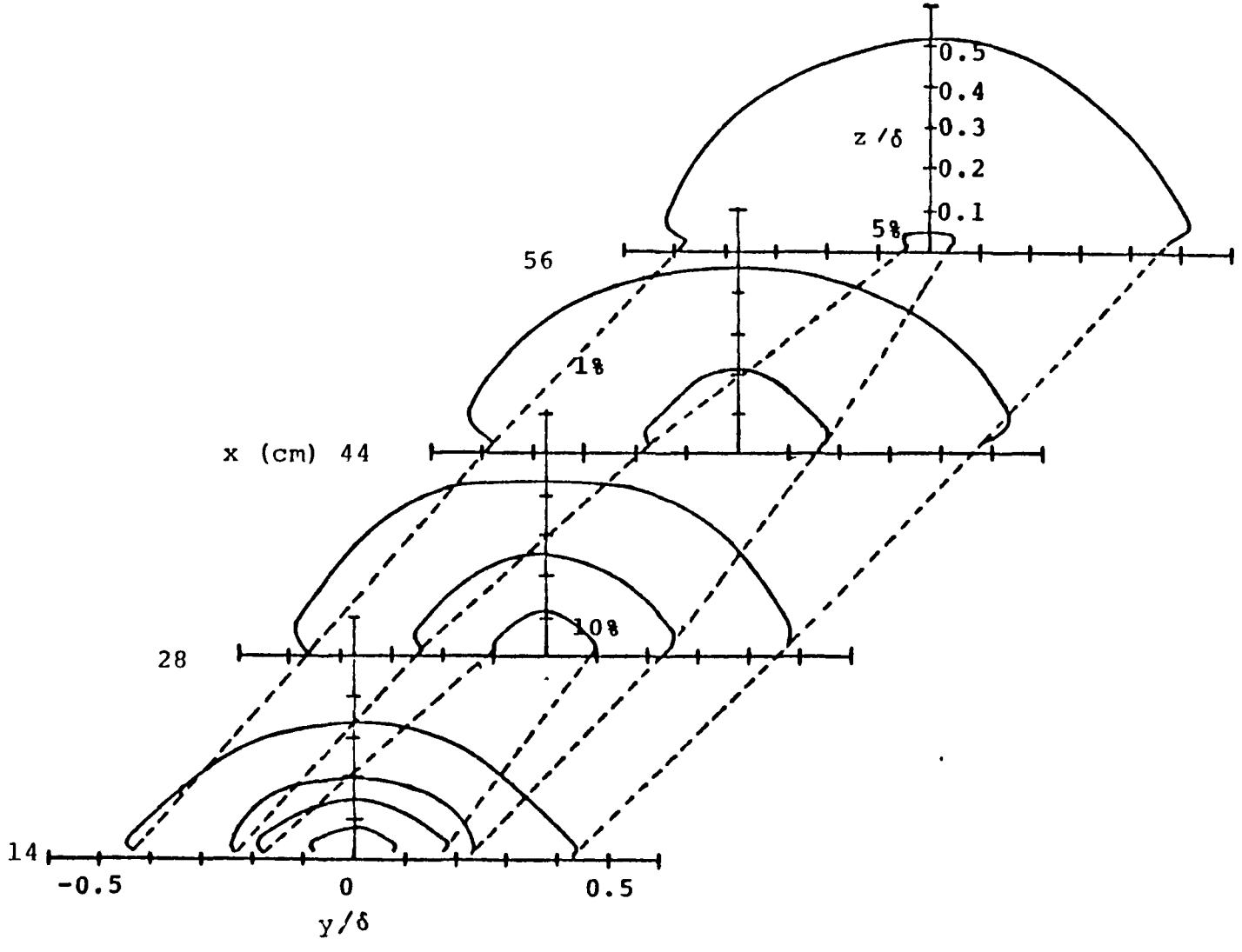

Figure 15. Helium Concentration Isoclines for Axial Line Source with Roughness Stage II.

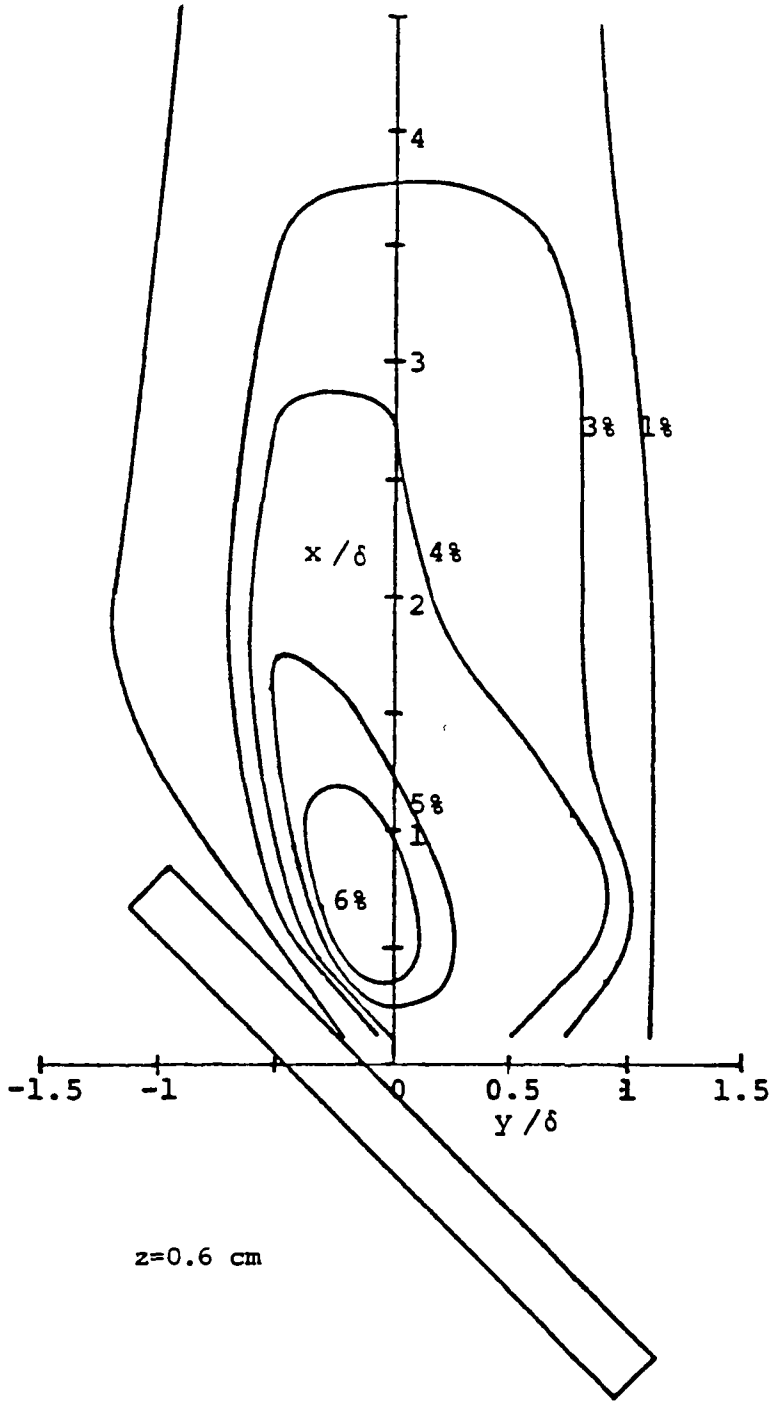

Figure 16. Helium Concentration Isoclines for Line Source at 45° from Transverse with Roughness, Stage II.

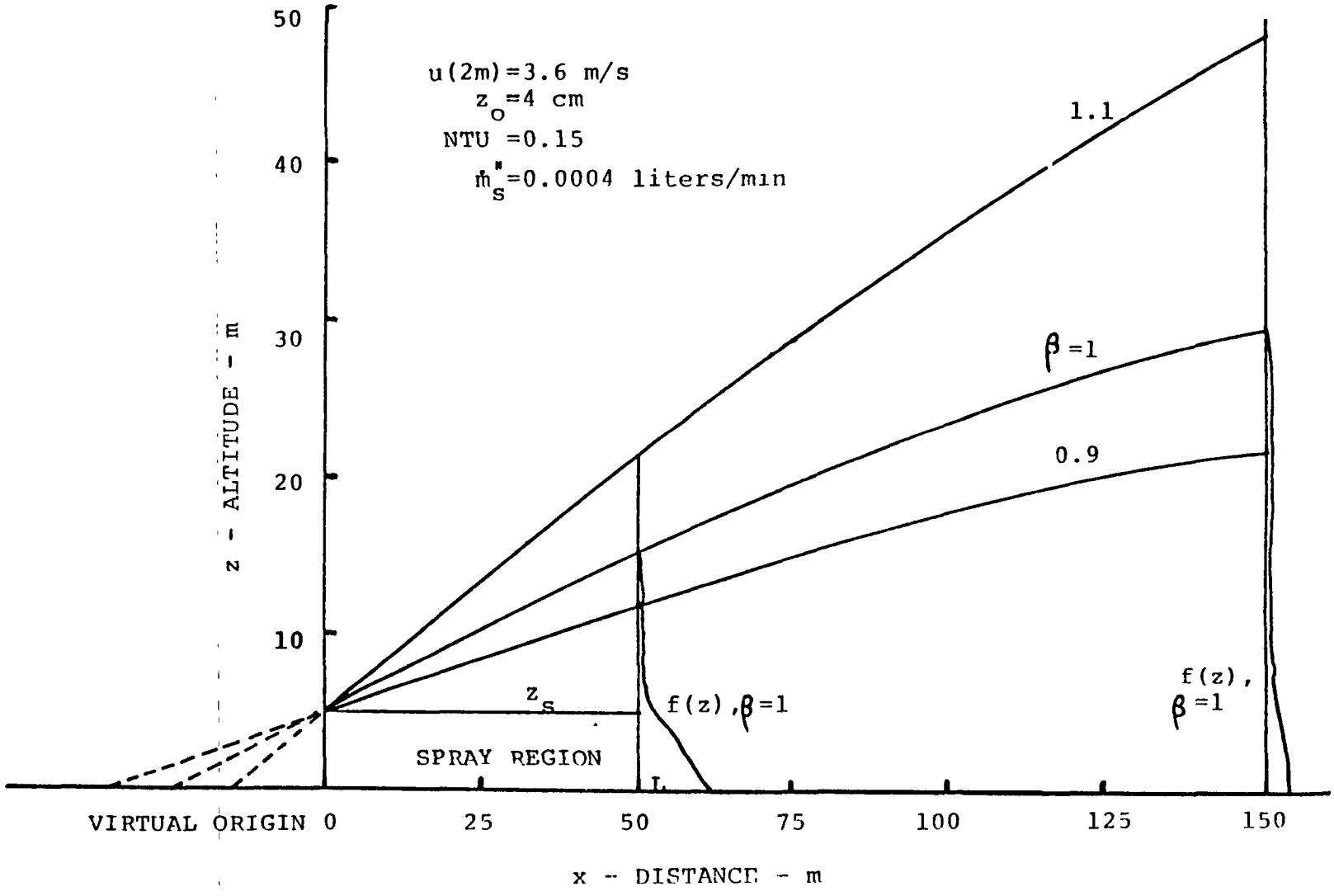

Figure 17. Numerical Results for Height of Discharge and Typical f Profiles in the Far Field, 4-Row Canal Configuration.

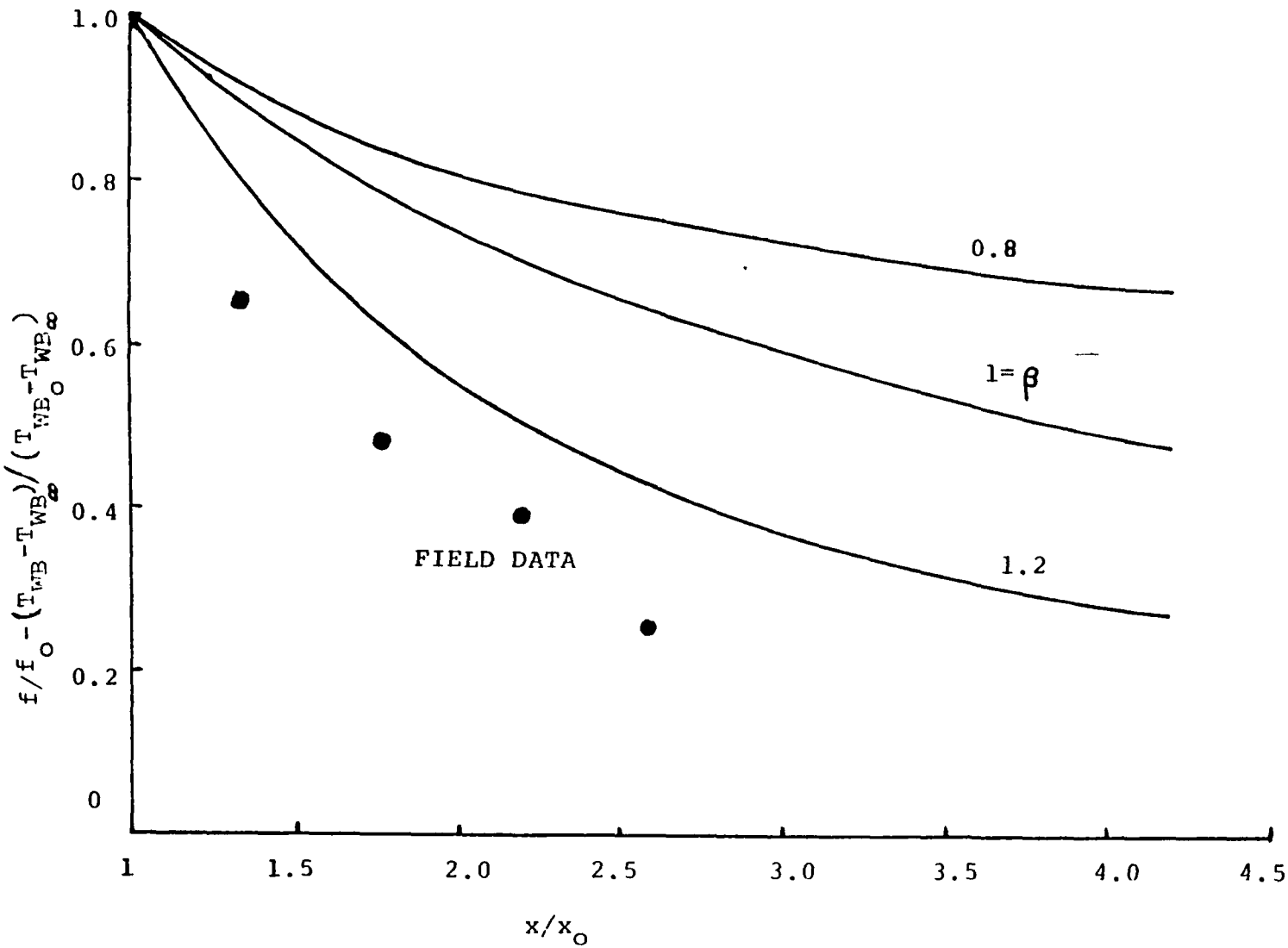

Figure 18. Numerical Results for Wet-Bulb Temperature Decay (Parameters of Figure 17).